ACS NANO

Cite This: ACS Nano 2017, 11, 10903-10913

www.acsnano.org

ARTICLE

Nanoscale Control over the Mixing Behavior of Surface-Confined Bicomponent Supramolecular Networks Using an Oriented External Electric Field

Gangamallaiah Velpula, Joan Teyssandier, Steven De Feyter,* and Kunal S. Mali*

Division of Molecular Imaging and Photonics, Department of Chemistry, KU Leuven-University of Leuven, Celestijnenlaan 200F, B-3001 Leuven, Belgium

Supporting Information

ABSTRACT: **Strong electric fields are known to influence the properties of molecules as well as materials. Here we show that by changing the orientation of an externally applied electric field, one can locally control the mixing behavior of two molecules physisorbed on a solid surface. Whether the starting two-component network evolves into an ordered two-dimensional (2D) cocrystal, yields an amorphous network where the two components phase separate, or shows preferential adsorption of only one component depends on the solution stoichiometry. The experiments are carried out by changing the orientation of the strong electric field that exists between the tip of a scanning tunneling microscope and a solid substrate. The structure of the two-component network typically changes from open porous at negative substrate bias to relatively compact when the polarity of the applied bias is reversed. The electric-field-induced mixing behavior is reversible, and the supramolecular system exhibits excellent stability and good response efficiency. When molecular guests are adsorbed in the porous networks, the field-induced switching behavior was found to be completely different. Plausible reasons behind the field-induced mixing behavior are discussed.**

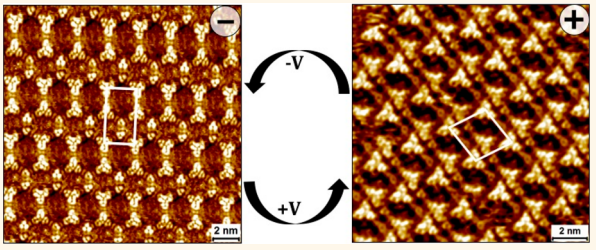

KEYWORDS: *electric-field-induced switching, mixing behavior, self-assembly, scanning tunneling microscopy, liquid−solid interface*

Electrostatic forces define most chemical and biological processes. Chemical reactions involve rearrangement of charges and electric fields associated with those charges. The stabilization of charged intermediates under given experimental conditions often determines the reactivity of chemical processes. In fact, reaction rates of a number of electrochemical processes are controlled by an applied electrical potential gradient. Natural systems also use electrostatic forces in a number of different ways. The high catalytic efficiency of enzymes is ascribed to their ability to stabilize charged transition states by using precisely positioned, preorganized polar functional groups within the active site. The efficiency of enzyme catalysis is intimately correlated with the magnitude of the electrostatic field exerted by its active site. The influence of local electric fields on the stabilization or destabilization of reaction intermediates is also invoked for explaining chemical catalysis.[1,2]

Although intensively harnessed by natural systems, the use of external electric fields (EEFs) to control chemical processes is one of the most underdeveloped strategies in synthetic chemistry. The idea that EEFs could be used to influence the outcome of chemical reactions is exciting because if one could use EEFs instead of ionic species as catalysts, it would be possible to manipulate a broad range of reactions. While the ability to control reaction rates using EEFs is often associated with redox systems, recent theoretical studies suggest that, if oriented precisely with respect to the reaction center, EEFs can potentially alter the course of chemical reactions even for nonredox processes.[3] This is because many covalent species have minor charge-separated contributors and EEFs awaken these dormant ionic structures.[4] EEFs are thus capable of manipulating the kinetics and/or thermodynamics of chemical reactions. It has been argued recently that oriented EEFs have the potential to be used as smart reagents for chemical reactions.[1]

For EEFs to be effective, the orientation of the field with respect to the chemical bonds is crucial.[4] This poses a major challenge for the evolution of the concept since orienting the field in precise directions and/or fixing the molecules in specific orientations is not straightforward. A scanning tunneling

Received: July 2, 2017
Accepted: October 11, 2017
Published: November 7, 2017

DOI: 10.1021/acsnano.7b04610
ACS Nano 2017, 11, 10903−10913

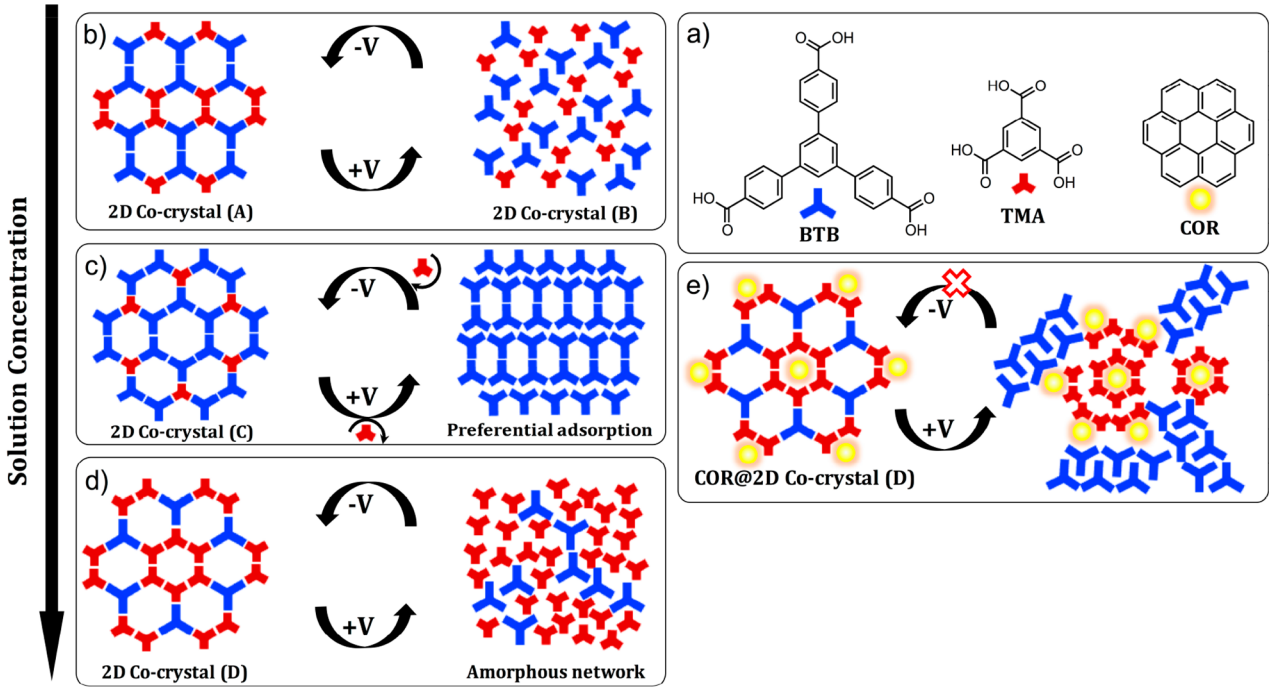

Figure 1. Schematic illustration of the nanoscale control over the mixing behavior of two molecules using EEF. (a) Molecular structures of 1,3,5-tri(4-carboxyphenyl)benzene (BTB), trimesic acid (TMA), and coronene (COR). (b–d) Schematics showing the influence of the surface composition on the outcome of the EEF-induced switching behavior. The surface composition in turn depends on the concentration of the two components in solution, which increases from (b) to (d). (e) Schematic showing the difference in the EEF-induced mixing behavior in the presence of guest against that observed in the absence of guest (see panel (d) for comparison).

microscope (STM), where an extremely strong electric field exists between a sharp metallic tip and a flat conductive surface, provides a seamless experimental setup to study the influence of EEFs on (supra)molecular systems. Due to the atomically sharp nature of the STM tip and a few-angstrom-wide gap between the tip and the substrate, a highly localized and directional electric field can be applied to systems positioned in this tunnel junction. Given the vanishingly small gap between the two electrodes, an electric field strength as high as $\sim 10^9$ V/m is considered normal under typical experimental conditions.[5]

In a recent example, an STM setup was used to study EEF-induced catalysis of Diels–Alder reaction.[6] The issue of specific orientation of the reagents with respect to the EEF was resolved by attaching the diene to the STM tip and by forming a chemisorbed self-assembled monolayer of the dienophile on a gold surface. Application of a voltage difference between the tip and the gold surface and moving the tip closer to the surface generated a tunneling current, which indicated the formation of the product in the tunnel junction. The frequency of product formation was studied using the break-junction (B-J) technique,[7] which provided a statistically relevant reaction rate. A 5-fold increase in the frequency of Diels–Alder adduct formation was observed in the presence of the oriented electric field, which ensures electron flow from the dienophile to the diene. This study demonstrated that carbon–carbon bond formation is accelerated in the presence of an oriented EEF.[6]

EEFs exhibit a range of different effects on molecular systems. The most commonly known effect is the shifting and splitting of spectral lines of atoms and molecules in the presence of EEFs, known as the Stark effect.[8] Electric-field-induced orientation of liquid-crystalline materials is a widely studied phenomenon that has already found a number of applications in day-to-day life.[9] It has been predicted that if an in-plane homogeneous electric field is applied across zigzag edges of graphene nanoribbons, the electrical current can be completely spin polarized.[10] Reversible *trans–cis* isomerization of single azobenzene derivatives was achieved using the electric field applied between an STM tip and a Au(111) surface.[11] The electric field in an STM setup was also used to induce reversible transitions in physisorbed monolayers[12−15] and for triggering formation of physisorbed bilayers.[16,17] Precisely defined movement of single molecular motors across an unmodified Cu surface was achieved using voltage pulses applied to the STM tip.[18] Recently, the tip of an STM has been employed to carry out a deacetylation reaction in a spatially controlled manner without significantly affecting the rest of the self-assembled monolayer, thereby allowing writing and reading of information at the nanoscale using molecular ink.[19]

In this contribution, we demonstrate yet another application of oriented EEFs. We show that by reversing the direction of the strong electric field that exists between the STM tip and a conductive solid substrate, one can locally control the mixing behavior of two molecules physisorbed on the surface. The experiment is carried out at the interface of an organic solution and highly oriented pyrolytic graphite (HOPG). When a solution containing a mixture of the two molecules in appropriate stoichiometry is deposited on HOPG, a crystalline, bicomponent supramolecular network with open voids is obtained. Starting with such a porous crystalline network at negative substrate bias, the constitution and topology of the supramolecular surface can be interchanged in a reversible fashion by simply flipping the substrate polarity. Whether the two molecules mix to yield an ordered crystalline network, or phase separate into an amorphous network, or show preferential adsorption of only one component at opposite substrate polarity is determined by the starting surface

DOI: 10.1021/acsnano.7b04610
ACS Nano 2017, 11, 10903–10913

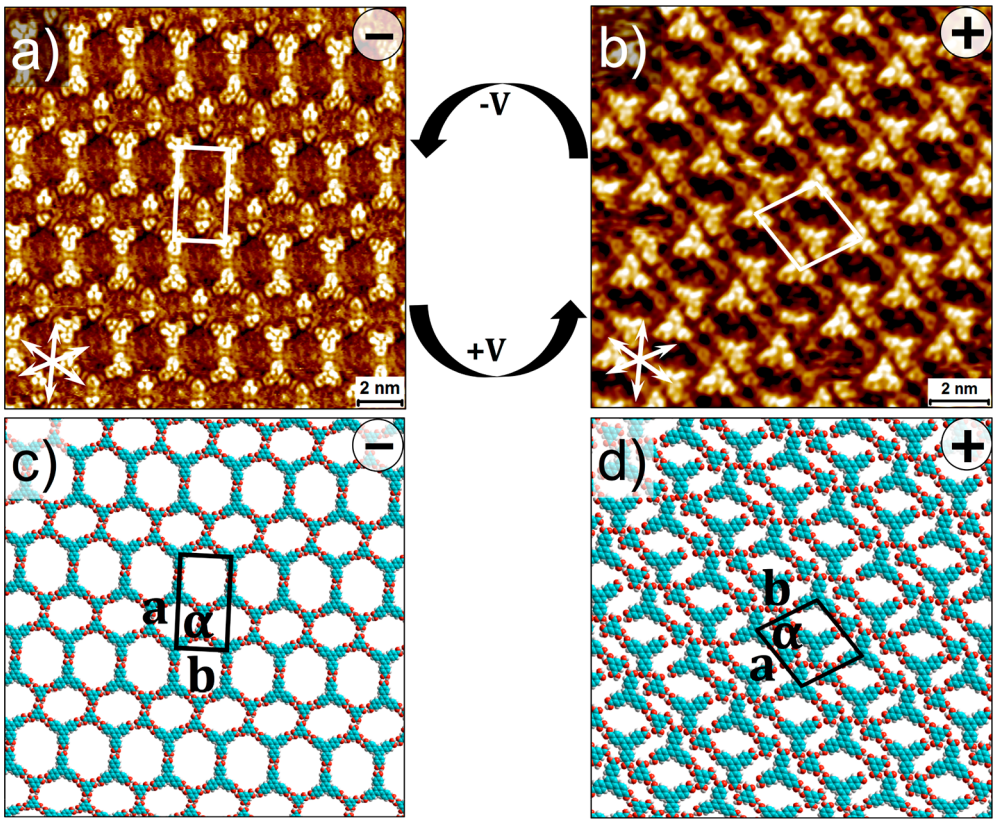

Figure 2. Reversible 2D cocrystal to 2D cocrystal transition in BTB−TMA mixed monolayers achieved by reversing the polarity of the substrate bias (C_{BTB} = 4.7 × 10^{-5} M; C_{TMA} = 3.2 × 10^{-4} M). Panels (a) and (b) show STM images of the 2D cocrystals A and B formed at negative and positive substrate polarity, respectively. Panels (c) and (d) show molecular models corresponding to the STM images provided in (a) and (b), respectively. Graphite symmetry axes are indicated in lower left corner of STM images. Imaging parameters: (a) I_{set} = 90 pA, V_{bias} = −1.0 V; (b) I_{set} = 90 pA, V_{bias} = 1.0 V. Unit cell parameters are provided in Table 1. For a large-scale STM image of cocrystal A see Figure S1 in the Supporting Information.

composition of the network, which in turn is dictated by the stoichiometry of the two molecules in solution. The outcome of the field-induced switching can be altered by incorporating guest molecules in the porous bicomponent network formed initially, in which case no switching is observed (Figure 1). We also discuss plausible mechanistic aspects of this EEF-induced switching behavior. The present investigation enriches the realm of EEF-induced chemical processes, which could potentially alter the way making and breaking of bonds is considered.

RESULTS AND DISCUSSION

Figure 1a shows the molecular structures of the building blocks used in this study. Both 1,3,5-tri(4-carboxyphenyl)benzene (BTB) and trimesic acid (TMA) are archetypal building blocks that assemble *via* $R^2_2(8)$ hydrogen bonding between carboxylic groups, and both yield a honeycomb porous network under typical experimental conditions when adsorbed independently.[20−23] Furthermore, when mixed in appropriate stoichiometry in solution, the two molecules form mixed self-assembled networks. Three different crystalline, open porous monolayer phases are obtained at the heptanoic acid (HA)/HOPG interface.[24] All three cocrystalline phases are stabilized via $R^2_2(8)$ hydrogen bonding between carboxylic groups of BTB and TMA. We used these perfectly crystalline arrangements as a model system to study the mixing behavior of molecules under varying electric field polarity. In the following paragraphs, we describe how the fate of the three crystalline arrangements changes when the substrate bias is reversed from negative to positive.

2D Cocrystal → 2D Cocrystal. Using relatively dilute solutions of the two components in HA, a perfectly crystalline mixed monolayer of BTB−TMA is obtained at negative substrate bias. Figure 2a shows a high-resolution STM image of the mixed monolayer formed at the HA/HOPG interface at negative sample bias, hereafter called 2D cocrystal A. Figure 2c displays a molecular model for cocrystal A built using the lattice parameters obtained from calibrated STM images. The network consists of hydrogen bonded homomeric dimers of BTB and TMA further connected to each other *via* heteromeric $R^2_2(8)$ hydrogen bonding. This ring synthon $R^x_y(Z)$ describes the characteristic association mode of aromatic carboxylic acids, where x and y are the number of H-bond donor and acceptor centers and Z is the total number of atoms in the ring. The unit cell is rectangular and contains two molecules of BTB and TMA each. Changing the orientation of the electric field by reversing the polarity of the applied sample bias leads to a structural transition. A relatively compact, crystalline two-component network is formed at positive substrate bias (Figure 2b). The unit cell of this phase, hereafter called 2D cocrystal B, is oblique and also contains two molecules of BTB and TMA each. Figure 2d shows the corresponding molecular model. In contrast to the model for cocrystal A, where the relative arrangement of the two molecules can be easily understood based on $R^2_2(8)$ hydrogen bonding, the relative positions of BTB and TMA in cocrystal B do not clearly reveal how the

DOI: 10.1021/acsnano.7b04610
ACS Nano 2017, 11, 10903−10913

Table 1. Structural Parameters of the Different Monolayer Phases Obtained upon Reversible Switching[a]

Negative substrate bias							Positive substrate bias					
System	Unit cell parameters			ρ	N		System	Unit cell parameters			ρ	N
	a (nm)	b (nm)	α (°)					a (nm)	b (nm)	α (°)		
Co-crystal (A)	4.2 ± 0.1	2.4 ± 0.1	90 ± 1	0.4	2 BTB, 2 TMA	Fast⇆Slow	Co-crystal (B)	2.5 ± 0.1	2.5 ± 0.1	78 ± 1	0.7	2 BTB, 2 TMA
Co-crystal (C)	5.7 ± 0.1	5.7 ± 0.1	60 ± 1	0.3	6 BTB, 2 TMA	Fast⇆Fast	BTB	3.3 ± 0.1	1.8 ± 0.1	74 ± 1	0.4	2 BTB
Co-crystal (D)	4.2 ± 0.1	4.2 ± 0.1	60 ± 1	0.5	2 BTB, 6 TMA	Fast⇆Slow	Amorphous BTB + TMA	-	-	-	-	-

[a] ρ = density (molecules/nm^2), N = molecules/unit cell.

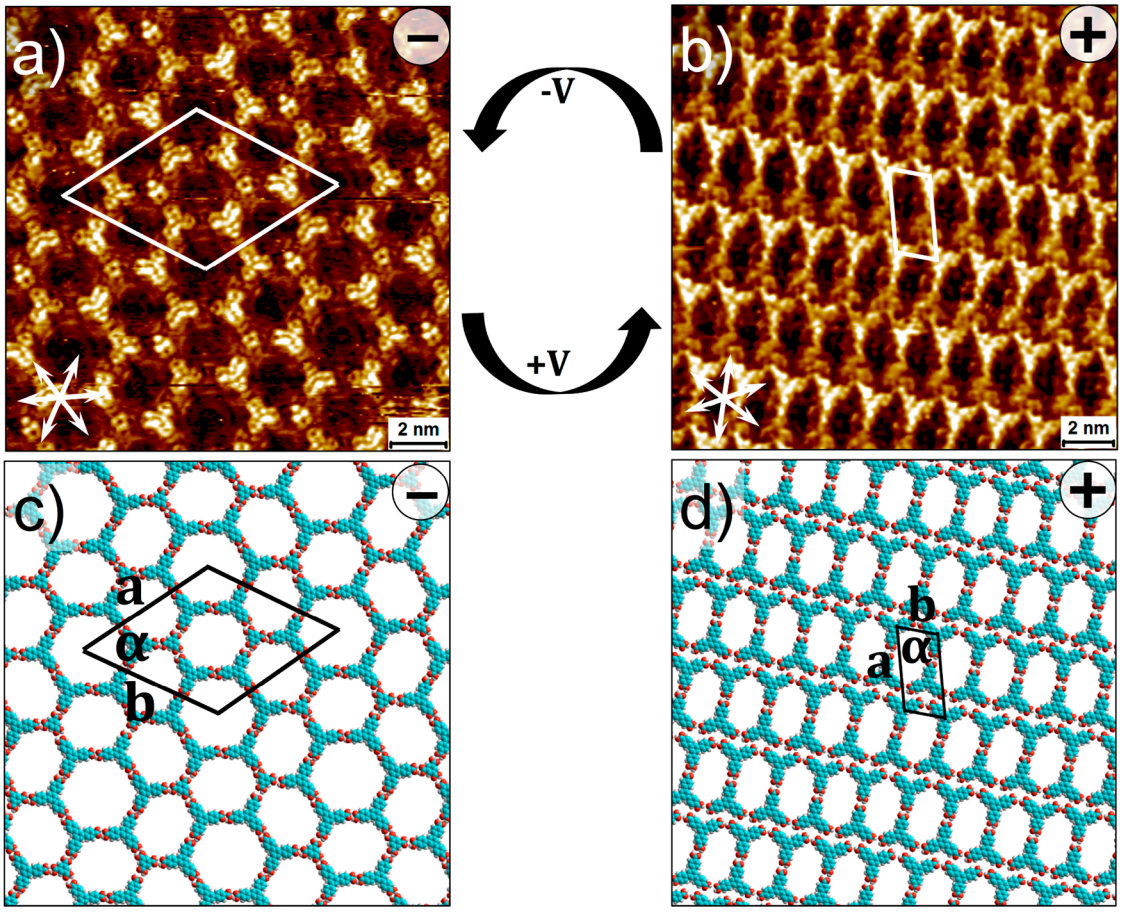

Figure 3. Reversible transition between 2D cocrystal C and preferentially adsorbed BTB network achieved by reversing the polarity of the substrate bias (C_{BTB} = 7.0 × 10^{-5} M; C_{TMA} = 2.4 × 10^{-4} M). Panels (a) and (b) show STM images of the 2D cocrystal C and the BTB network formed at negative and positive substrate polarity, respectively. Panels (c) and (d) show molecular models corresponding to the STM images provided in (a) and (b), respectively. Graphite symmetry axes are indicated in the lower left corner of the STM images. Imaging parameters: (a) I_{set} = 90 pA, V_{bias} = −1.0 V; (b) I_{set} = 90 pA, V_{bias} = 1.0 V. Unit cell parameters are provided in Table 1. For a large-scale STM image of the 2D cocrystal C see Figure S4 in the Supporting Information.

molecules interact with each other. In the model proposed in Figure 2d, the positions of the two molecules are accurately reproduced; however their relative orientation is somewhat tentative. At first glance the ordered compact network obtained at positive substrate bias appears to be sustained by a combination of heteromeric $R^2_2(8)$ hydrogen bonding between BTB and TMA (*vide infra*) and relatively weak aromatic −C−H---O= interactions between the BTB−BTB and BTB−TMA molecules. Based on the molecular arrangement, it appears that there is partial disruption of the original $R^2_2(8)$ hydrogen bonding at positive substrate bias.

The time-dependence of all structural transitions discussed here was evaluated by considering the outcome of the switching immediately after reversing the bias and also after 10 min of

DOI: 10.1021/acsnano.7b04610
ACS Nano 2017, 11, 10903−10913

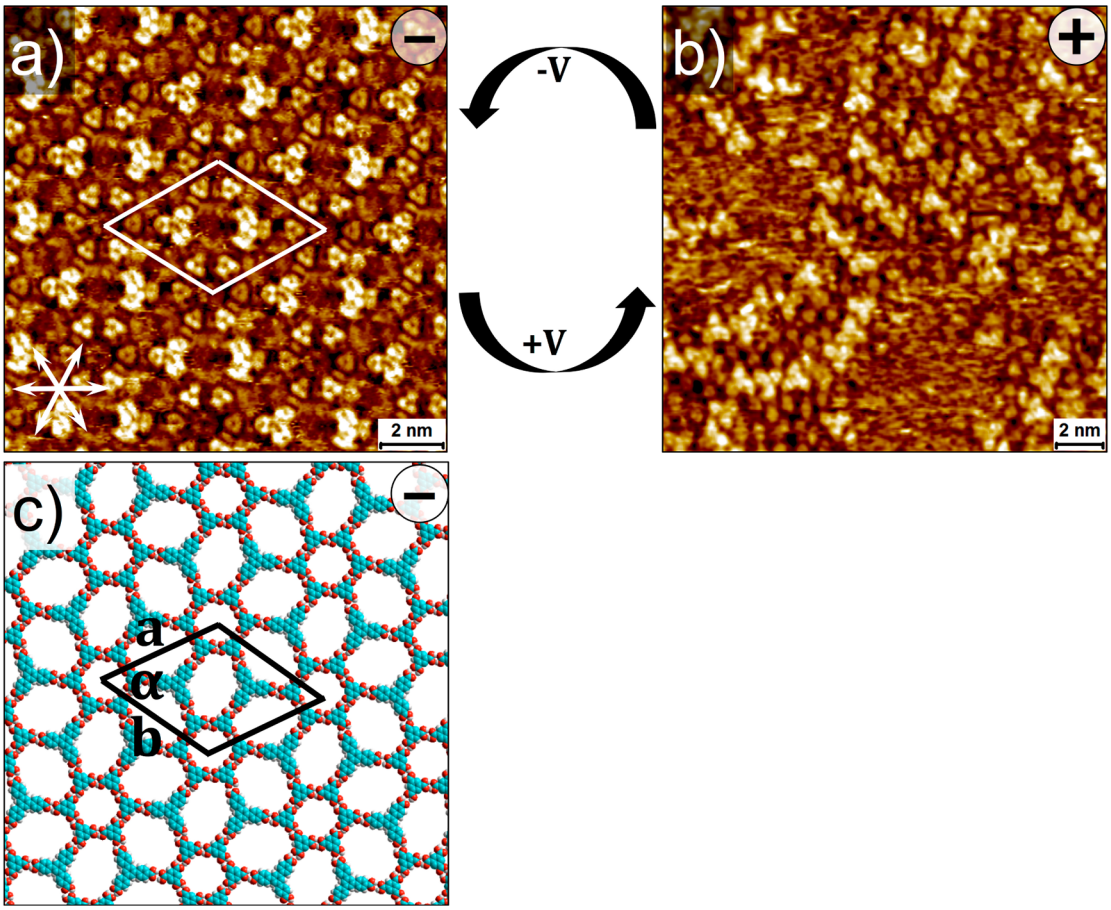

Figure 4. Reversible transition between 2D cocrystal D and an amorphous network comprising both BTB and TMA achieved by reversing the polarity of the substrate bias (C_{BTB} = 2.5 × 10^{-4} M and C_{TMA} = 1.7 × 10^{-3} M). Panels (a) and (b) show STM images of the 2D cocrystal D and the amorphous network formed at negative and positive substrate polarity, respectively. Panel (c) shows a molecular model corresponding to the STM image provided in (a). Imaging parameters: (a) I_{set} = 90 pA, V_{bias} = −1.0 V; (b) I_{set} = 90 pA, V_{bias} = 1.0 V. Unit cell parameters are provided in Table 1. For a large-scale STM image of cocrystal D see Figure S6 in the Supporting Information.

scanning the surface continuously at a given (reversed) polarity. Based on this consideration, this 2D cocrystal to 2D cocrystal structural transition is relatively sluggish because only a few isolated small domains of 2D cocrystal B were observed immediately after reversing the polarity. The system evolves into a long-range-ordered network only after further continuous scanning of the same area at positive substrate bias for ∼10 min. Electric-field-induced structural transitions for the parent BTB network (alone), however, were found to be almost instantaneous, wherein the network changes from one scan line to the other upon reversing the polarity.[13,14] Despite its sluggishness in the forward direction, the transition in the BTB−TMA network described above is fully reversible and can be initiated by reversing the substrate bias back to negative. Although the opposite transformation is almost instantaneous, sometimes the network obtained immediately after the polarity switch is that of cocrystal C, which transitions into the cocrystal A in the subsequent scan. Large, well-ordered domains of 2D cocrystal A are obtained with virtually no defects after continuously scanning the area for 10 min (for time-dependence of the transitions see Figure S2 and Figure S3 in the Supporting Information).

2D Cocrystal → BTB (Preferential Adsorption). An increase in the concentration of the two components in solution yields a bicomponent supramolecular network with hexagonal symmetry at negative substrate bias, hereafter called 2D cocrystal C. Figure 3a shows an STM image of the network, which consists of alternating hexagons made up of only BTB molecules and four molecules of BTB and two molecules of TMA, respectively. The unit cell is relatively large and contains two molecules of TMA and six molecules of BTB. Figure 3c provides a molecular model corresponding to the STM image. It reveals that, similar to cocrystal A, this network is also sustained by homomeric and heteromeric $R^2_2(8)$ hydrogen bonding between BTB and BTB−TMA molecules, respectively. Reversal of the substrate bias led to appearance of another phase, which is entirely composed of BTB molecules (Figure 3b). The unit cell of this phase is oblique and consists of two BTB molecules. The molecular model provided in Figure 3d reveals that dimeric rows of BTB molecules are stabilized by a combination of regular $R^2_2(8)$ hydrogen bonding (*vide infra*), lateral hydrogen bonding interactions between carboxyl groups of adjacent BTB molecules within the same dimer row, and possibly also weak aromatic −C−H---O═C− hydrogen bonding between molecules that belong to adjacent rows. This is clearly a case of preferential adsorption of BTB over TMA at positive values of substrate bias. The polarity switch expels the TMA molecules from the HOPG surface. The reverse transition, however, reaccommodates the TMA molecules back into the network, thereby furnishing back the original 2D cocrystal C. Notably, the forward as well as the reverse transitions in this case are virtually instantaneous with

DOI: 10.1021/acsnano.7b04610
ACS Nano 2017, 11, 10903−10913

changes in the network observed within a few scan lines after the reversal in bias polarity (see Figure S5 in the Supporting Information). Thus, in contrast to the previous case, the outcome of this switching experiment is almost the same immediately after the reversal of the substrate polarity and after continuous scanning of the same area for 10 min.

2D Cocrystal → Amorphous Network. Further increase in the concentration of the two components in HA solution yielded another bicomponent network with hexagonal symmetry. 2D cocrystal D is formed at negative substrate bias and consists of alternating hexagons made up of only TMA molecules and four TMA and two BTB molecules, respectively (Figure 4a). The unit cell contains six molecules of TMA and two molecules of BTB. Thus, this network features the exact opposite arrangement of BTB and TMA molecules within the lattice in comparison to that in cocrystal C. Similar to the two previous cocrystal networks observed at negative polarities, this network is also stabilized by homomeric and heteromeric $R^2_2(8)$ hydrogen bonds between the two molecules (Figure 4c). Reversing the substrate bias lead to formation of an amorphous network as shown in Figure 4b. This network features randomly distributed BTB as well as TMA molecules. No structural order evolved even after scanning the surface for 10 min. In fact, the amorphous structure persists even after scanning the same area for much longer times (~2 h). Similar to other monolayer phases described above, the opposite transition occurs readily, furnishing ordered domains of cocrystal D (for time-dependence, see Figure S7 in the Supporting Information).

The experimental results described above clearly reveal that open, crystalline bicomponent phases are stabilized at negative substrate bias, whereas relatively compact networks survive at positive substrate bias. The precise outcome of the EEF-induced switching, *i.e.*, whether the system forms another 2D cocrystal, shows preferential adsorption of one component, or leads to formation of an amorphous monolayer phase, depends on the starting surface composition. It can be readily noticed that all the networks formed at negative substrate bias are stabilized by head-to-head $R^2_2(8)$ hydrogen bonding, whereas the ones obtained by reversing the substrate bias show partial or complete disruption of the $R^2_2(8)$ hydrogen bonds. BTB and TMA molecules appear to adsorb in a planar conformation in the monolayer phases observed at positive as well as negative substrate bias. This brings us to an important question: What is the influence of the polarity switch at the level of single molecule? In the following paragraphs we attempt to divulge the different possibilities.

Mechanistic Aspects. Monolayer phases of the parent BTB system can be reversibly switched between different states by using two types of external stimuli: thermal[25,26] and EEF.[13,14] Thermally induced structural transitions in the BTB network have been studied both under UHV conditions[25] and at the solution−solid interface.[26] The porous honeycomb network of BTB formed under UHV conditions on a Ag(111) surface undergoes two structural transitions wherein the initial open porous network transforms into successively more compact structures. The onset of a Shockley surface state monitored from dI/dV spectroscopy for each network indicated the presence of gradually increasing negative charge on the surface consistent with deprotonated carboxyl groups. Thus, thermally induced deprotonation of the carboxylic groups was proposed to be the driving force behind the structural transitions in the BTB network.[25] It must be noted that the first transition occurs at only 320 K, indicating a relatively facile deprotonation process. Similar temperature-induced deprotonation behavior has been reported for TMA adsorbed on a Ag(111) surface.[27]

A second hypothesis was proposed on the basis of EEF-induced switching observed in a BTB network at the nonanoic acid/HOPG interface.[13] It was hypothesized that the alignment of the molecular dipole with respect to the electric field upon reversing the direction of applied bias is responsible for the observed structural transitions. It must be noted that optimization of the BTB molecular structure in this work[13] was carried out under vacuum, which allows free rotation of the carboxyphenyl rings. The molecule, however, adsorbs in a planar conformation on the graphite surface, and the planar conformation does not have any net dipole moment. The authors claimed that this mechanism is also compatible with the formation of partially deprotonated BTB species at positive values of substrate bias that can be assisted by water traces. The typical organic solvents used for STM experiments are often stored under ambient conditions and thus may contain several parts per million of water. The water molecules can act as proton acceptors and thus drive the transition to the compact structure at positive values of substrate bias. This combined information indicates that the electric field alignment of the molecular dipole may not be sufficient to explain the EEF-induced structural transitions in BTB monolayers, and the partial deprotonation of BTB at positive substrate bias cannot be ruled out.

In order to evaluate which mechanism is consonant with the present system, we attempted to assess the fate of TMA upon reversal in the substrate bias. Since TMA is a small rigid molecule, it is not expected to exhibit any dipole moment arising due to free rotation of phenyl rings as observed for BTB. Besides, it is well-known that the carboxyl groups of TMA (as well as BTB) form in-plane hydrogen bonds upon adsorption on the surface of HOPG, meaning that the hydrogen bonds and thus the carboxyl group itself are coplanar with the rest of the aromatic framework. Experimental results clearly reveal that the honeycomb network of TMA obtained at negative substrate bias changes into a densely packed network that consists of rows of TMA molecules when the substrate bias is reversed (Supporting Information Figure S8). This network can be switched back to the original honeycomb structure by reversing the polarity of the substrate bias. We note that the structural transitions in the TMA network are sporadic, meaning that there are instances when the network does not change immediately upon changing the polarity of the substrate bias. While the exact origin of this irregular switching process is not clear, it could be related to the relatively smaller difference in the packing densities of the two networks obtained at opposite substrate polarities.

Although the discussion provided above alludes to partial deprotonation of the carboxylic acid groups as the reason underlying the observed transitions, we agree that the arguments provided are fairly circumstantial. It has been contended in the past that prediction of supramolecular networks cannot exclusively be based on formation of ideal intermolecular hydrogen bonds because certain aromatic carboxylic acids are known to disfavor regular $R^2_2(8)$ hydrogen bonding due to packing constraints.[28,29] Notwithstanding these aspects, theoretical studies provide ample indication that covalent bond cleavage is possible under high electric fields (~10^9 V/m) that exist at the tip−sample junction in an STM

DOI: 10.1021/acsnano.7b04610
ACS Nano 2017, 11, 10903−10913

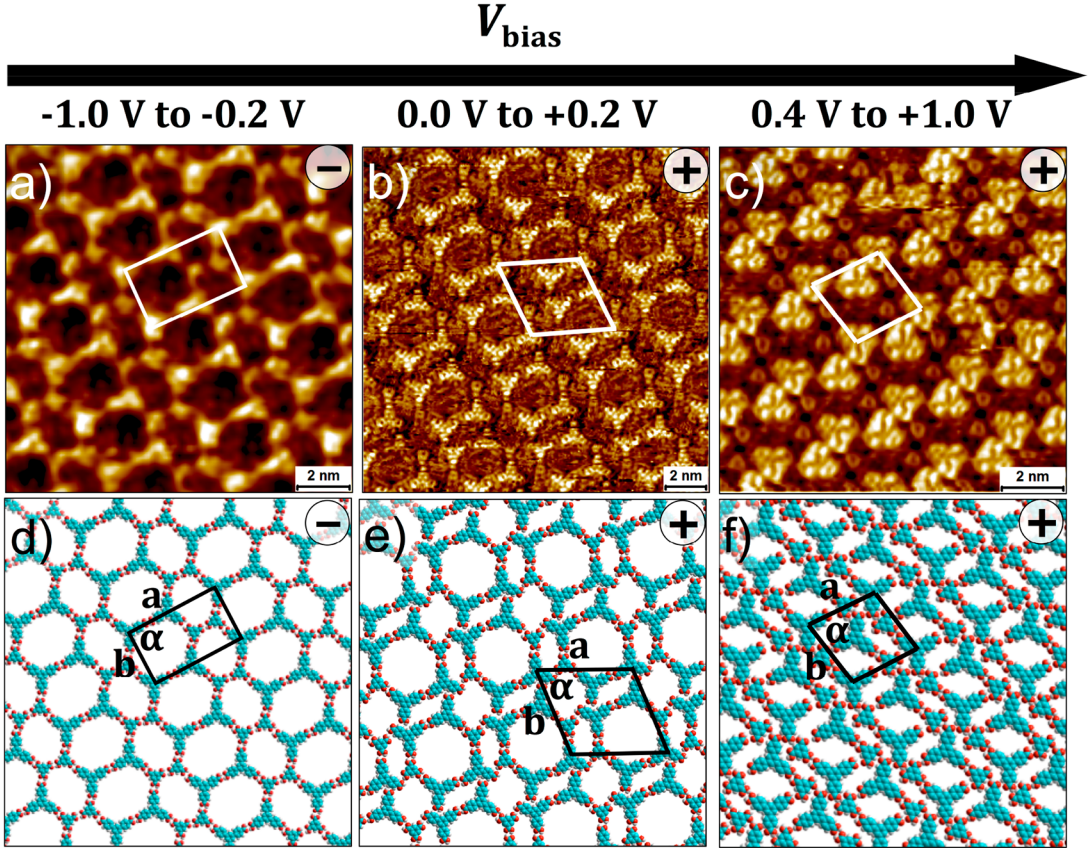

Figure 5. Voltage-magnitude-dependent STM images showing the gradual transition of cocrystal A (a) to cocrystal B (c) *via* cocrystal E (b). Panels (d)−(f) show corresponding molecular models. Unit cell parameters for cocrystal (E) are $a = 4.2 \pm 0.1$ nm, $b = 4.2 \pm 0.2$ nm, and $\alpha = 74 \pm 2°$. Tunneling current (a−c) $I_{set} = 60$ pA.

setup.[1,4] Many formally covalent bonds possess minor charge-separated resonance contributors. It has been suggested that an electric field is capable of electrostatically stabilizing such ionic forms and thus may result in overall stabilization of an alternative (supra)molecular structure.[30] In such a scenario, the presence of high EEF ensures that the ionic structure energetically crosses over below the covalent structure, thus eventually leading to bond cleavage.[31] It must be noted that a number of these calculations were carried out on homonuclear diatomic molecules such as H_2, N_2, O_2, F_2, Cl_2, *etc*. Compared to these, the current system involves a relatively polar −O−H bond with a readily dissociable proton. Thus, it is not unreasonable to assume partial deprotonation of the molecules at positive substrate bias. The behavior of the C−Cl bond, which is a relatively polar bond, under EEFs is particularly interesting in this context and is in line with the present experimental results. These bonds show enhanced ionicity when the EEF is oriented in one direction, and in the reverse EEF direction, the ionicity is quenched.[1,4,30]

Besides its polarity, the magnitude of the substrate bias also controls the composition of the monolayer phases. In the experiments described so far, only the sign of the substrate bias was changed from negative to positive and *vice versa* (typically from −1 to +1 V). A threshold for the observed structural transitions was discovered when the substrate bias was changed gradually in increments of 200 mV from −1 to +1 V. Figure 5 shows voltage magnitude-dependent structural transitions in the case of cocrystal A. 2D cocrystal A remains stable in the voltage window of −1.0 to −0.2 V (Figure 5a). Further changes in the substrate bias lead to formation of another cocrystal network, which remains stable within the voltage range of 0.0 to 0.2 V (cocrystal E, Figure 5b). Additional increase in the field strength furnished the final structure in the form of cocrystal B, which remains stable within the voltage window of 0.4 to 1.0 V (Figure 5c). The anatomy of cocrystal E is consistent with disruption of hydrogen bonding between two TMA molecules in the original structure. The magnitude dependence of the transition can thus alternatively be understood by considering gradual deprotonation of the TMA molecules as a function of increase in the field strength on the positive side of the substrate bias. These systematic measurements reveal that neither of the supramolecular networks observed at positive (+1 V) or negative (−1 V) bias are stable at or around 0 V when the field is weak or completely removed. The observation of the distorted network indicating partial disruption of regular hydrogen bonding between the two molecules indicates that the partially deprotonated species may be present on the surface at or around zero field.

At first sight it appears rather counterintuitive that the networks change from open porous at negative bias to compact at positive bias. This is because, if one assumes partial deprotonation of the molecules, then one expects repulsive interactions within the network formed at positive bias. While this is true to a large extent, it must be noted that all the open porous networks discussed here are sustained by six hydrogen bonds per molecule. Despite their open nature, which does not conform to the thermodynamic principle of close-packing, the stability of such networks is governed by maximization of

DOI: 10.1021/acsnano.7b04610
ACS Nano 2017, 11, 10903−10913

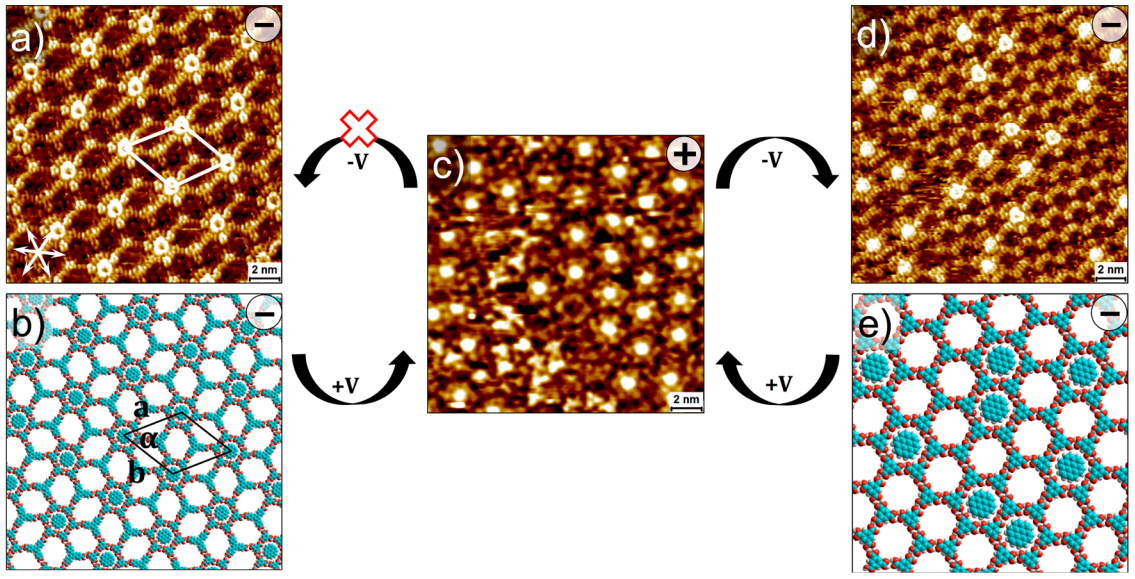

Figure 6. Influence of guest molecules on EEF-induced structural transitions. (a) STM image of the three-component system obtained by adding COR to a preformed monolayer of cocrystal D. COR molecules selectively occupy the small hexagonal cavities. (b) Molecular model corresponding to the STM image provided in (a). (c) STM image of the network obtained after reversing the polarity. This network resembles the flower structure of the TMA with very low surface coverage of BTB molecules that form an amorphous network in between the TMA–COR host–guest structure. This network does not revert back to the original three-component BTB–TMA–COR system upon reversing the substrate bias to negative. Instead, it leads to formation of a TMA–COR host–guest network (d, e) wherein TMA forms a regular honeycomb network. (For a large-scale image of the three-component system and for the time-dependence of the transition see Supporting Information Figure S9 and Figure S10, respectively.)

energy per molecule, in which case each molecule forms six energetically favorable hydrogen bonds with its neighbor. Disruption of such $R^2_2(8)$ hydrogen bonding is expected to significantly reduce the stability of the open porous network. Under such circumstances, not only the overall energy of the supramolecular surface is determined by close packing wherein the energy per unit area dominates, but the carboxylate ion formed after (partial) deprotonation may also engage in hydrogen bonding with intact carboxyl groups. A hydrogen bond formed between carboxylate ions and carboxyl groups is known to be extremely strong and is categorized as a low-barrier hydrogen bond (LBHB).[32−34] Such bonds are typically shorter (2.3−2.5 Å, bond strength ∼37 kcal/mol)[33] than regular hydrogen bonds (>2.6 Å, bond strength ∼7.4 kcal/mol)[35] formed between carboxyl groups. In the case of an LBHB, the hydrogen atom occupies a position approximately equidistant from the two oxygen atoms and is equally shared between the donor and the acceptor. The role of such strong ionic hydrogen bonds in stabilizing reaction intermediates within the active sites of enzymes is an intensely debated topic.[33,36] Carboxylates are discussed prominently in this context because all negative charges on proteins are carboxylates.[32,37,38] Based on these aspects, it is not unreasonable to consider formation of strong hydrogen bonds between the carboxylate anions and carboxyl groups which may contribute to the overall stabilization of the networks formed at positive substrate bias. This means that the apparent carboxyl−carboxyl contacts present in the networks obtained at positive bias (*vide supra*) could as well be ascribed to carboxyl−carboxylate hydrogen bonding instead of regular $R^2_2(8)$ carboxyl−carboxyl hydrogen bonding. The chemical insensitivity of scanning tunneling microscopy precludes the determination of the exact sites where the plausible deprotonation has occurred. Nevertheless, the structures formed at positive substrate bias can be interpreted by considering the aforementioned carboxylate−carboxyl hydrogen bonding, and hypothetical models based on such consideration can be found in the Supporting Information (Figures S11 and S12).

Host−Guest System: Coronene@Cocrystal D. Finally, we tested how the presence of guest molecules affects the EEF-induced phase behavior in BTB−TMA monolayers. We have recently demonstrated the potential use of a similar switching process for controlled release and capture of molecular guests at the solution−solid interface.[14] EEF-induced porous to compact transitions in the BTB network were used to "squeeze" out guest molecules adsorbed in its open cavities. The two polycyclic aromatic molecules, namely, coronene and nanographene, adsorb in the host cavities of the BTB network at negative substrate polarity and could be expelled out of the network by reversing the polarity, which leads to formation of the compact network. The presence of guest molecules did not impede the process, and the EEF-induced structural transitions in the BTB network were found to proceed as readily as that in the absence of guest molecules. A recent study also found similar behavior where the structural transitions in the BTB network were barely slowed down by incorporation of a variety of different guest molecules.[39]

Cocrystal D was chosen to evaluate the impact of guest molecules on the switching process, as it features well-ordered TMA hexagons within the lattice that are known to be ideal host cavities for COR.[40] Addition of a droplet of COR dissolved in HA to a preformed monolayer of cocrystal D resulted in formation of a perfectly ordered, three-component host−guest network where COR occupies the TMA hexagons. A similar result is obtained upon premixing the three components in solution. The STM image provided in Figure 6a clearly shows the presence of COR as bright disc-shaped

DOI: 10.1021/acsnano.7b04610
ACS Nano 2017, 11, 10903−10913

features inside the TMA cavities. The adsorption of COR neither changes the lattice parameters nor changes the way BTB and TMA interact with each other. Reversing the polarity led to a somewhat unusual outcome wherein the host–guest network consisting of TMA and COR remains on the surface with markedly reduced surface coverage of BTB at positive polarity. TMA forms the "flower" structure[20] at positive substrate bias with a few COR molecules incorporated in the hexagonal cavities. It must be noted that in the absence of COR this system evolves into an amorphous network at positive substrate bias (see Figure 4). What is even more interesting is that further reversal of the substrate bias to negative values does not furnish the initial three-component host–guest system. Instead, a regular honeycomb network of TMA with COR guests is obtained with virtually complete removal of BTB from the scanned surface. Further scanning the same area at negative substrate polarity does not change the surface composition. Thus, the reversibility of the structural transition is completely altered in the presence of COR molecules, which preferentially stabilize the TMA network due to ideal host–guest interactions at both positive and negative substrate bias. This is an interesting case where an otherwise (thermodynamically) stable cocrystal is converted into a metastable state upon EEF-induced switching (also see Figure S9 in the Supporting Information). Similar behavior was observed in the case of porous networks formed by TMA and 4,4′-bipyridine. When COR was introduced into the system, 4,4′-bipyridine was removed from the surface with exclusive formation of a TMA–COR network.[41]

CONCLUSIONS AND OUTLOOK

Using a combination of supramolecular chemistry, surface science, and STM, we have described above how changing the orientation of a strong, highly localized electric field affects the mixing behavior of two molecules adsorbed at the solution–solid interface within the tunneling junction. Two molecules that form cocrystalline physisorbed monolayers based on hydrogen bonding interactions between carboxyl groups respond in a reversible fashion to the change in the direction of an EEF. The starting surface composition dictates the final outcome upon reversing the field direction. We essentially show that by using EEFs one can control, in a spatially controlled fashion, how two molecules interact with each other. The approach presented here illustrates yet another interesting manifestation of strong EEFs on (supra)molecular systems.

While the highly resolved STM data clearly show drastic changes in the structure and composition of the supramolecular networks in response to changes in the orientation of the EEF, pinpointing the exact reason behind those changes is not straightforward due to the extremely localized nature of the process. We have discussed two possibilities, namely, changes in the surface dipole and partial deprotonation of the molecules. We note that the two mechanisms are not mutually exclusive. We hypothesize that EEF-induced partial deprotonation of the two molecules could be the reason behind the field-controlled mixing behavior. This hypothesis is supported by recent theoretical studies that indicate that strong EEFs influence bond energy and are thus capable of causing bond cleavage. Although STM is an excellent experimental tool to study EEF-induced processes, we concede that it is limited by its lack of chemical sensitivity. While a number of mechanistic details still need to be verified experimentally, this work provides a compelling example of electric-field-controlled mixing behavior of surface-adsorbed supramolecular systems.

Experimental study of strong EEF-induced processes at the single-molecule level is still a fairly unchartered territory, and a number of aspects remain unknown. The influence of the EEF in the present case is localized within a few square nanometers underneath the STM tip. Alternative strategies are needed in order to carry out EEF-induced chemical reactions on a preparative scale, which will determine if EEF-induced processes could be profitably employed in synthesis and/or separation technology. For a fundamental understanding of chemical changes occurring in such systems in response to EEFs, a combination of spectroscopy and microscopy needs to be employed. Further attempts to find evidence of deprotonation in the current system are underway using tip-enhanced Raman spectroscopy.

EXPERIMENTAL SECTION

Commercially available BTB (Aldrich 98+%), TMA (98%), COR (Aldrich 97%), and heptanoic acid (Sigma-Aldrich ≥99%) were used as received. Stock solutions of BTB (1.4×10^{-3} M), TMA (4.8×10^{-3} M), and COR (2.0×10^{-3} M) were prepared by dissolving an appropriate amount of solid in 1-heptanoic acid. The stock solutions were diluted further to make concentration series. All STM experiments were performed at room temperature (21–23 °C) using a PicoLE (Agilent) machine operating in constant-current mode with the tip immersed in the supernatant liquid. STM tips were prepared by mechanically cutting a Pt/Ir wire (80%/20%, diameter 0.2 mm). Prior to imaging, a drop of solution was placed onto a freshly cleaved surface of highly oriented pyrolytic graphite (grade ZYB, Advanced Ceramics Inc., Cleveland, OH, USA). The experiments were repeated in two or three sessions using different tips to check for reproducibility and to avoid experimental artifacts, if any. For analysis purposes, recording of a monolayer image was followed by imaging the graphite substrate underneath it under the same experimental conditions, except for increasing the current and lowering the bias. Raw STM images of the molecular monolayers were calibrated by using the STM images of the HOPG lattice obtained immediately after recording the monolayer image as a reference. This exercise removes the distortions in the STM images that arise due to thermal drift. The lattice parameters of bimolecular monolayer were then obtained from these calibrated images. Scanning probe image processor (SPIP) software (Image Metrology ApS) was used for image calibration. The unit cell parameters were determined by examining at least four images, and only the average values are reported. The images are Gaussian filtered. The imaging parameters are indicated in the figure caption: tunneling current (I_{set}) and sample bias (V_{bias}). After the determination of the unit cell from drift-corrected STM images, a molecular model of the observed monolayer was constructed using the HyperChem Professional 7.5 program. First, a molecular model for each single molecule was built, and then this model was geometry optimized under vacuum using molecular mechanics optimization (Fletcher–Reeves algorithm with an RMS gradient of 0.1 kcal/Å mol). Following this, a 2D crystal based on unit cell parameters obtained from calibrated STM images was built by duplicating, translating, and rotating the molecules at the lattice sites. The orientation of adjacent molecules with respect to each other was defined on the basis of supramolecular intuition and prior knowledge on carboxylic acid self-assembly from published literature.

ASSOCIATED CONTENT

Supporting Information

The Supporting Information is available free of charge on the ACS Publications website at DOI: 10.1021/acsnano.7b04610.

Large-scale STM images, time-lapse STM images showing the time-dependence of the phase transitions,

DOI: 10.1021/acsnano.7b04610
ACS Nano 2017, 11, 10903–10913

and STM images showing the phase transition in the TMA system (PDF)

AUTHOR INFORMATION

Corresponding Authors

*E-mail: steven.defeyter@kuleuven.be.
*E-mail: kunal.mali@kuleuven.be.

ORCID

Gangamallaiah Velpula: 0000-0002-0642-6892
Joan Teyssandier: 0000-0003-4369-0542
Steven De Feyter: 0000-0002-0909-9292
Kunal S. Mali: 0000-0002-9938-6446

Notes

The authors declare no competing financial interest.

ACKNOWLEDGMENTS

G.V. acknowledges the award of a Marie Sklodowska-Curie individual fellowship (number 706314, GRAPHIL). This work is supported by the Fund of Scientific Research–Flanders (FWO), KU Leuven–Internal Funds, Belgian Federal Science Policy Office (IAP-7/05), and European Research Council under the European Union's Seventh Framework Programme (FP7/2007–2013)/ERC Grant Agreement No. 340324.

REFERENCES

(1) Shaik, S.; Mandal, D.; Ramanan, R. Oriented Electric Fields as Future Smart Reagents in Chemistry. *Nat. Chem.* **2016**, *8*, 1091–1098.
(2) Boxer, S. G.; Fried, S. D. Electric Fields and Enzyme Catalysis. *Annu. Rev. Biochem.* **2017**, *86*, 387–415.
(3) Corrales, M. E.; González-Vázquez, J.; Balerdi, G.; Solá, I. R.; de Nalda, R.; Bañares, L. Control of Ultrafast Molecular Photodissociation by Laser-Field-Induced Potentials. *Nat. Chem.* **2014**, *6*, 785–790.
(4) Sowlati-Hashjin, S.; Matta, C. F. The Chemical Bond in External Electric Fields: Energies, Geometries, and Vibrational Stark Shifts of Diatomic Molecules. *J. Chem. Phys.* **2013**, *139*, 144101.
(5) Hong, Y. A.; Hahn, J. R.; Kang, H. Electron Transfer Through Interfacial Water Layer Studied by Scanning Tunneling Microscopy. *J. Chem. Phys.* **1998**, *108*, 4367–4370.
(6) Aragonès, A. C.; Haworth, N. L.; Darwish, N.; Ciampi, S.; Bloomfield, N. J.; Wallace, G. G.; Diez-Perez, I.; Coote, M. L. Electrostatic Catalysis of a Diels–Alder Reaction. *Nature* **2016**, *531*, 88–91.
(7) Xiang, D.; Wang, X.; Jia, C.; Lee, T.; Guo, X. Molecular-Scale Electronics: From Concept to Function. *Chem. Rev.* **2016**, *116*, 4318–4440.
(8) Boxer, S. G. Stark Realities. *J. Phys. Chem. B* **2009**, *113*, 2972–2983.
(9) Yang, D.-K.; Wu, S.-T. *Effects of Electric Field on Liquid Crystals. In Fundamentals of Liquid Crystal Devices*; John Wiley & Sons, Ltd, 2014; pp 127–148.
(10) Son, Y.-W.; Cohen, M. L.; Louie, S. G. Half-Metallic Graphene Nanoribbons. *Nature* **2006**, *444*, 347–349.
(11) Alemani, M.; Peters, M. V.; Hecht, S.; Rieder, K.-H.; Moresco, F.; Grill, L. Electric Field-Induced Isomerization of Azobenzene by STM. *J. Am. Chem. Soc.* **2006**, *128*, 14446–14447.
(12) Mali, K. S.; Wu, D.; Feng, X.; Müllen, K.; Van der Auweraer, M.; De Feyter, S. Scanning Tunneling Microscopy-Induced Reversible Phase Transformation in the Two-Dimensional Crystal of a Positively Charged Discotic Polycyclic Aromatic Hydrocarbon. *J. Am. Chem. Soc.* **2011**, *133*, 5686–5688.
(13) Cometto, F. P.; Kern, K.; Lingenfelder, M. Local Conformational Switching of Supramolecular Networks at the Solid/Liquid Interface. *ACS Nano* **2015**, *9*, 5544–5550.
(14) Lee, S.-L.; Fang, Y.; Velpula, G.; Cometto, F. P.; Lingenfelder, M.; Müllen, K.; Mali, K. S.; De Feyter, S. Reversible Local and Global Switching in Multicomponent Supramolecular Networks: Controlled Guest Release and Capture at the Solution/Solid Interface. *ACS Nano* **2015**, *9*, 11608–11617.
(15) Lei, S.-B.; Deng, K.; Yang, Y.-L.; Zeng, Q.-D.; Wang, C.; Jiang, J.-Z. Electric Driven Molecular Switching of Asymmetric Tris-(phthalocyaninato) Lutetium Triple-Decker Complex at the Liquid/Solid Interface. *Nano Lett.* **2008**, *8*, 1836–1843.
(16) Zheng, Q.-N.; Liu, X.-H.; Liu, X.-R.; Chen, T.; Yan, H.-J.; Zhong, Y.-W.; Wang, D.; Wan, L.-J. Bilayer Molecular Assembly at a Solid/Liquid Interface as Triggered by a Mild Electric Field. *Angew. Chem., Int. Ed.* **2014**, *53*, 13395–13399.
(17) Cui, K.; Mali, K. S.; Ivasenko, O.; Wu, D.; Feng, X.; Walter, M.; Müllen, K.; De Feyter, S.; Mertens, S. F. L. Squeezing, Then Stacking: From Breathing Pores to Three-Dimensional Ionic Self-Assembly under Electrochemical Control. *Angew. Chem., Int. Ed.* **2014**, *53*, 12951–12954.
(18) Kudernac, T.; Ruangsupapichat, N.; Parschau, M.; Macia, B.; Katsonis, N.; Harutyunyan, S. R.; Ernst, K.-H.; Feringa, B. L. Electrically Driven Directional Motion of a Four-Wheeled Molecule on a Metal Surface. *Nature* **2011**, *479*, 208–211.
(19) Lindner, M.; Valášek, M.; Mayor, M.; Frauhammer, T.; Wulfhekel, W.; Gerhard, L. Molecular Graph Paper. *Angew. Chem., Int. Ed.* **2017**, *56*, 8290–8294.
(20) Griessl, S.; Lackinger, M.; Edelwirth, M.; Hietschold, M.; Heckl, W. Heckl Self-Assembled Two-Dimensional Molecular Host-Guest Architectures From Trimesic Acid. *Single Mol.* **2002**, *3*, 25–31.
(21) Kampschulte, L.; Lackinger, M.; Maier, A.-K.; Kishore, R. S. K.; Griessl, S.; Schmittel, M.; Heckl, W. M. Solvent Induced Polymorphism in Supramolecular 1,3,5-Benzenetribenzoic Acid Monolayers. *J. Phys. Chem. B* **2006**, *110*, 10829–10836.
(22) Lackinger, M.; Griessl, S.; Heckl, W. M.; Hietschold, M.; Flynn, G. W. Self-Assembly of Trimesic Acid at the Liquid–Solid Interface a Study of Solvent-Induced Polymorphism. *Langmuir* **2005**, *21*, 4984–4988.
(23) Lackinger, M.; Heckl, W. M. Carboxylic Acids: Versatile Building Blocks and Mediators for Two-Dimensional Supramolecular Self-Assembly. *Langmuir* **2009**, *25*, 11307–11321.
(24) Kampschulte, L.; Werblowsky, T. L.; Kishore, R. S. K.; Schmittel, M.; Heckl, W. M.; Lackinger, M. Thermodynamical Equilibrium of Binary Supramolecular Networks at the Liquid–Solid Interface. *J. Am. Chem. Soc.* **2008**, *130*, 8502–8507.
(25) Ruben, M.; Payer, D.; Landa, A.; Comisso, A.; Gattinoni, C.; Lin, N.; Collin, J.-P.; Sauvage, J.-P.; De Vita, A.; Kern, K. 2D Supramolecular Assemblies of Benzene-1,3,5-triyl-tribenzoic Acid: Temperature-Induced Phase Transformations and Hierarchical Organization with Macrocyclic Molecules. *J. Am. Chem. Soc.* **2006**, *128*, 15644–15651.
(26) Gutzler, R.; Sirtl, T.; Dienstmaier, J. r. F.; Mahata, K.; Heckl, W. M.; Schmittel, M.; Lackinger, M. Reversible Phase Transitions in Self-Assembled Monolayers at the Liquid–Solid Interface: Temperature-Controlled Opening and Closing of Nanopores. *J. Am. Chem. Soc.* **2010**, *132*, 5084–5090.
(27) Payer, D.; Comisso, A.; Dmitriev, A.; Strunskus, T.; Lin, N.; Wöll, C.; DeVita, A.; Barth, J. V.; Kern, K. Ionic Hydrogen Bonds Controlling Two-Dimensional Supramolecular Systems at a Metal Surface. *Chem. - Eur. J.* **2007**, *13*, 3900–3906.
(28) Dienstmaier, J. F.; Mahata, K.; Walch, H.; Heckl, W. M.; Schmittel, M.; Lackinger, M. On the Scalability of Supramolecular Networks – High Packing Density vs Optimized Hydrogen Bonds in Tricarboxylic Acid Monolayers. *Langmuir* **2010**, *26*, 10708–10716.
(29) MacLeod, J. M.; Ivasenko, O.; Perepichka, D. F.; Rosei, F. Stabilization of Exotic Minority Phases in a Multicomponent Self-Assembled Molecular Network. *Nanotechnology* **2007**, *18*, 424031.
(30) Karafiloglou, P. Control of Delocalization and Structural Changes by Means of an Electric Field. *J. Comput. Chem.* **2006**, *27*, 1883–1891.

DOI: 10.1021/acsnano.7b04610
ACS Nano 2017, 11, 10903–10913

(31) Schirmer, B.; Grimme, S. Electric Field Induced Activation of H2-Can DFT Do the Job? *Chem. Commun.* **2010**, *46*, 7942−7944.
(32) Lin, J.; Pozharski, E.; Wilson, M. A. Short Carboxylic Acid−Carboxylate Hydrogen Bonds Can Have Fully Localized Protons. *Biochemistry* **2017**, *56*, 391−402.
(33) Graham, J. D.; Buytendyk, A. M.; Wang, D.; Bowen, K. H.; Collins, K. D. Strong, Low-Barrier Hydrogen Bonds May Be Available to Enzymes. *Biochemistry* **2014**, *53*, 344−349.
(34) Warshel, A.; Papazyan, A.; Kollman, P. On Low-Barrier Hydrogen Bonds and Enzyme Catalysis. *Science* **1995**, *269*, 102−106.
(35) Steiner, T. The Hydrogen Bond in the Solid State. *Angew. Chem., Int. Ed.* **2002**, *41*, 48−76.
(36) Cleland, W. W.; Frey, P. A.; Gerlt, J. A. The Low Barrier Hydrogen Bond in Enzymatic Catalysis. *J. Biol. Chem.* **1998**, *273*, 25529−25532.
(37) Brück, A.; McCoy, L. L.; Kilway, K. V. Hydrogen Bonds in Carboxylic Acid−Carboxylate Systems in Solution. 1. In Anhydrous, Aprotic Media. *Org. Lett.* **2000**, *2*, 2007−2009.
(38) Smallwood, C. J.; McAllister, M. A. Characterization of Low-Barrier Hydrogen Bonds. 7. Relationship between Strength and Geometry of Short-Strong Hydrogen Bonds. The Formic Acid−Formate Anion Model System. An ab Initio and DFT Investigation. *J. Am. Chem. Soc.* **1997**, *119*, 11277−11281.
(39) Lee, S.-L.; Lin, C.-H.; Cheng, K.-Y.; Chen, Y.-C.; Chen, C.-H. Stability of Guest-Incorporated 2D Molecular Networks. *J. Phys. Chem. C* **2016**, *120*, 25505−25510.
(40) Griessl, S. J. H.; Lackinger, M.; Jamitzky, F.; Markert, T.; Hietschold, M.; Heckl, W. M. Incorporation and Manipulation of Coronene in an Organic Template Structure. *Langmuir* **2004**, *20*, 9403−9407.
(41) Li, M.; Xie, P.; Deng, K.; Yang, Y.-L.; Lei, S.-B.; Wei, Z.-Q.; Zeng, Q.-D.; Wang, C. A Dynamic Study of the Structural Change in the Binary Network in Response to Guest Inclusion. *Phys. Chem. Chem. Phys.* **2014**, *16*, 8778−8782.

DOI: 10.1021/acsnano.7b04610
ACS Nano 2017, 11, 10903−10913

Supporting information

Nanoscale Control over the Mixing Behavior of Surface-Confined Bi-Component Supramolecular Networks using an Oriented External Electric Field

Gangamallaiah Velpula, Joan Teyssandier, Steven De Feyter and Kunal S. Mali**

Division of Molecular Imaging and Photonics, Department of Chemistry, KU Leuven-University of Leuven, Celestijnenlaan 200F, B-3001 Leuven, Belgium

Corresponding authors: steven.defeyter@kuleuven.be, kunal.mali@kuleuven.be

Contents:

Experimental details: STM

Commercially available 1,3,5-tris(4-carboxyphenyl)benzene (BTB) (Aldrich 98+%), trimesic acid (TMA),)(98%) coronene (COR) (Aldrich 97%) and heptanoic acid (Sigma-Aldrich ≥ 99%) were used as received. Stock solutions of BTB (1.4×10^{-3} M), TMA (4.8×10^{-3} M) and coronene (2.0×10^{-3} M), were prepared by dissolving appropriate amount of solid in 1-heptanoic acid. The stock solutions were diluted further to make concentration series. All STM experiments were performed at room temperature (21–23^{0}C) using a PicoLE (Agilent) machine operating in constant-current mode with the tip immersed in the supernatant liquid. STM tips were prepared by mechanically cutting a Pt/Ir wire (80%/20%, diameter 0.2 mm). Prior to imaging, a drop of solution was placed onto a freshly cleaved surface of highly oriented pyrolytic graphite (HOPG, grade ZYB, Advanced Ceramics Inc., Cleveland, USA). The experiments were repeated in 2-3 sessions using different tips to check for reproducibility and to avoid experimental artefacts, if any. For analysis purposes, recording of a monolayer image was followed by imaging the graphite substrate underneath it under the same experimental conditions, except for increasing the current and the lowering the bias. The images were corrected for drift via Scanning Probe Image Processor (SPIP) software (Image Metrology ApS), using the recorded graphite images for calibration purposes, allowing a more accurate unit cell determination. The unit cell parameters were determined by examining at least 4 images and only the average values are reported. The images are Gaussian filtered. The imaging parameters are indicated in the figure caption: tunneling current (I_{set}), and sample bias (V_{bias}). The molecular models were built using Hyperchem™ 7.0 program.

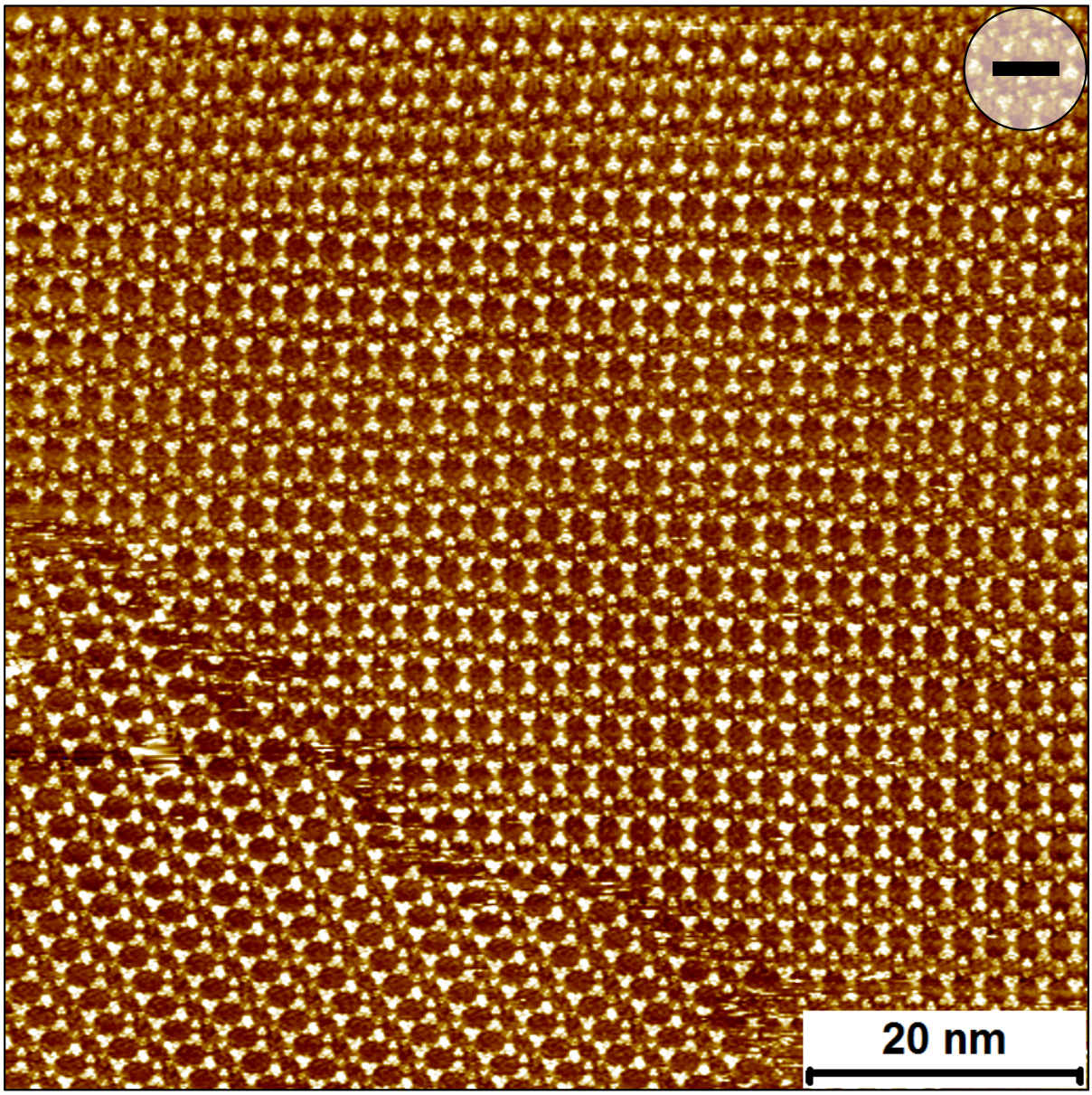

Figure S1. Large-scale STM image of 2D co-crystal (A) formed at negative values of substrate bias (C_{BTB} = 4.7 X 10^{-5} M and C_{TMA} = 3.2 X 10^{-4} M). Imaging parameters: I_{set} = 90 pA, V_{bias} = −1.0 V

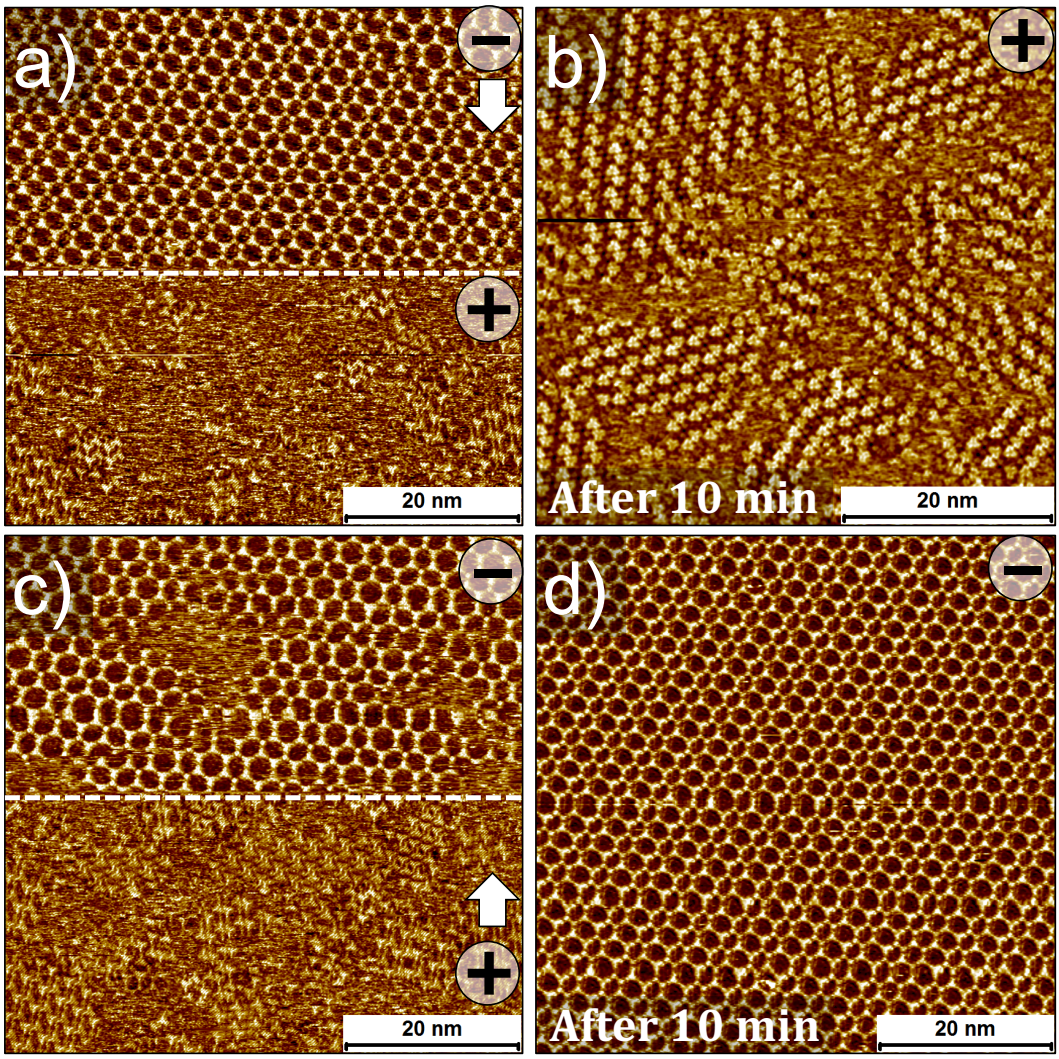

Figure S2. Influence of the reversal of substrate polarity on the mixing behavior studied immediately after, and upon 10 minutes of continuous scanning the same area. (a) STM image showing the changes in the structure of 2D co-crystal (A) upon reversing the polarity of the substrate bias from negative to positive, halfway (white dashed line) through the scan while keeping the magnitude of the bias as well as the tunneling current constant. The white arrow in the top-right corner depicts the scan direction. The part of the image scanned at positive substrate bias clearly shows the formation of isolated crystallites of 2D co-crystal (B). (b) STM image showing (approximately) the same area as in (a) scanned further continuously at positive substrate bias. Relatively larger, well-ordered domains of 2D co-crystal (B) are obtained. (c) STM image showing the reverse transition where domains of 2D co-crystal (C) are formed immediately upon reversing the polarity. This network changes readily into the starting co-crystal (A) in the subsequent scan. (d) The same area as in (c) scanned further at negative substrate bias for 10 minutes. Imaging parameters: I_{set} = 60 pA, V_{bias} = −/+1000 mV

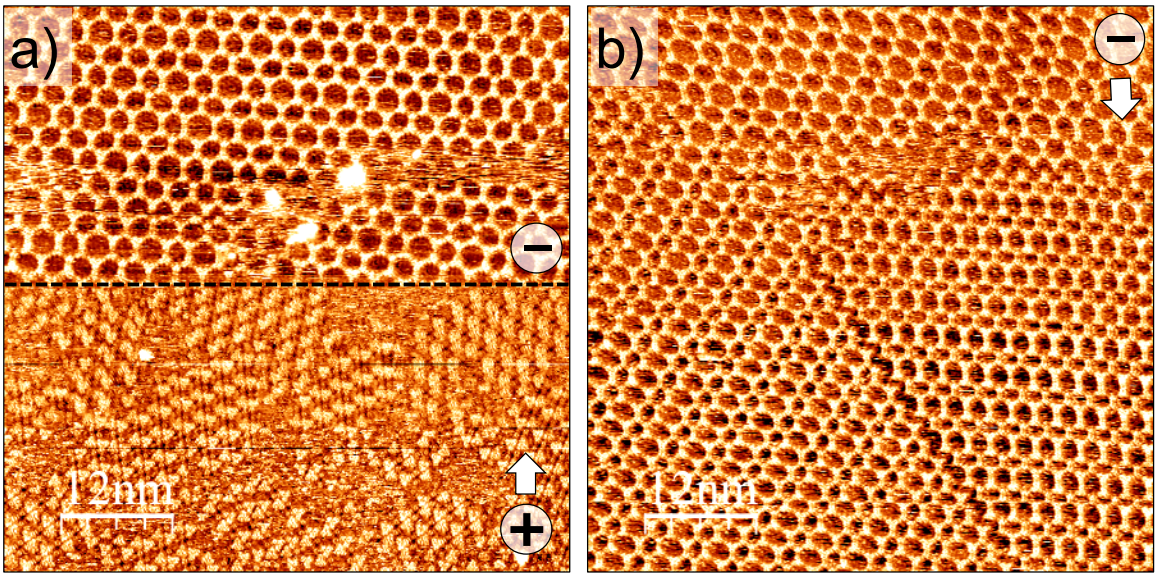

Figure S3. Two STM images obtained sequentially showing the transition of co-crystal (B) to co-crystal (A) via co-crystal (C). Note that the first transition, namely co-crystal (B) to co-crystal (C) is initiated by changing the polarity of substrate bias whereas the second transition is spontaneous. (a) STM image showing the transition of co-crystal (B) into co-crystal (C) in response to change in the polarity of the substrate bias. The bias was reversed approximately halfway (black dotted line) through the image. The formation of co-crystal (C) instead of co-crystal (A) is clearly evident (see upper half of panel a). (b) STM image showing spontaneous transition of co-crystal (C) into co-crystal (A). In the upper half of the image, arrangement of molecules clearly resembles that in co-crystal (C) whereas which changes to co-crystal (A) (see lower half of panel b).

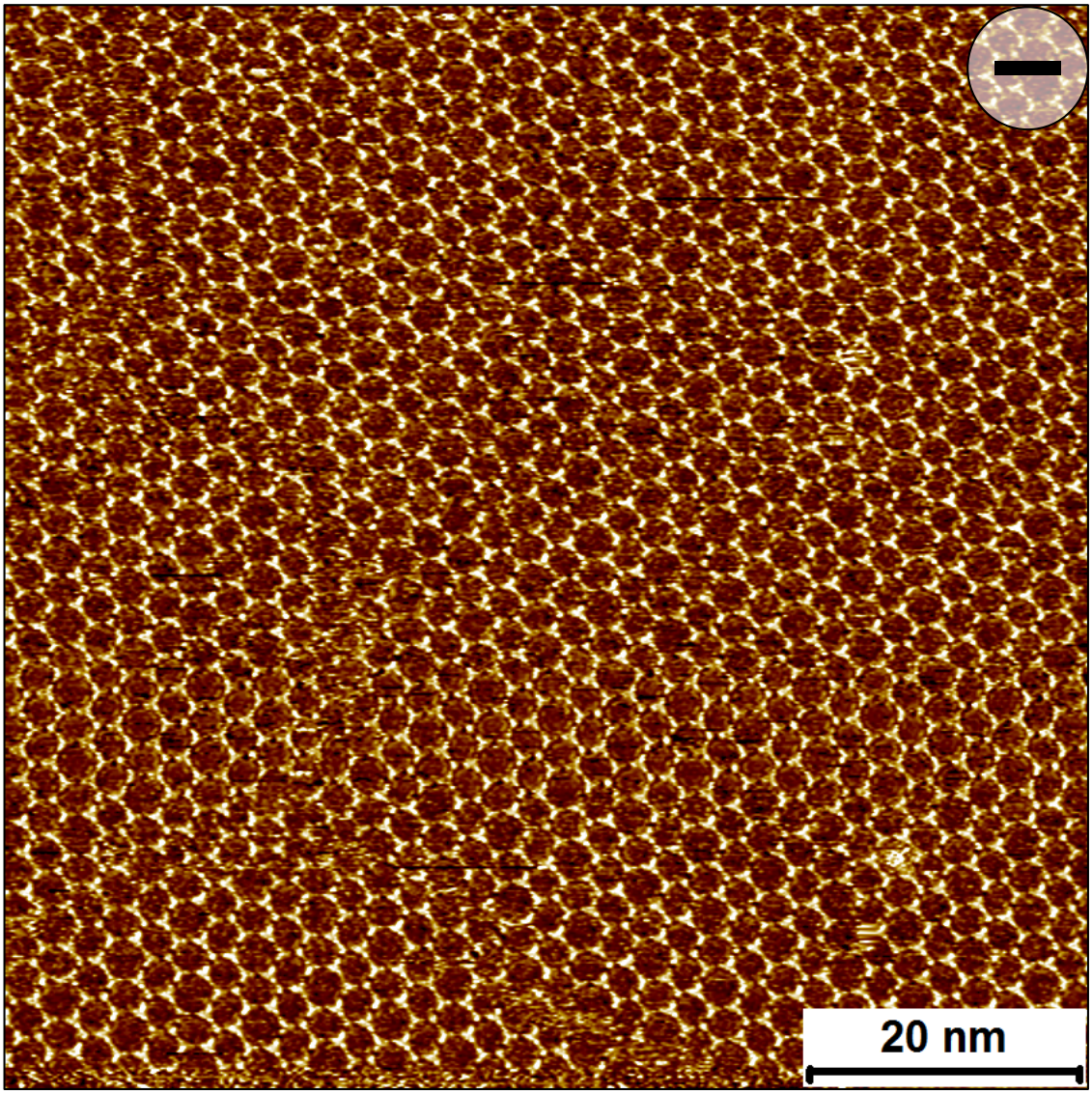

Figure S4. Large-scale STM image of 2D co-crystal (C) formed at negative values of substrate bias. (C_{BTB} = 7.0 X 10^{-5} M and C_{TMA} = 2.4 X 10^{-4} M) Imaging parameters: I_{set} = 90 pA, V_{bias} = –1.0 V

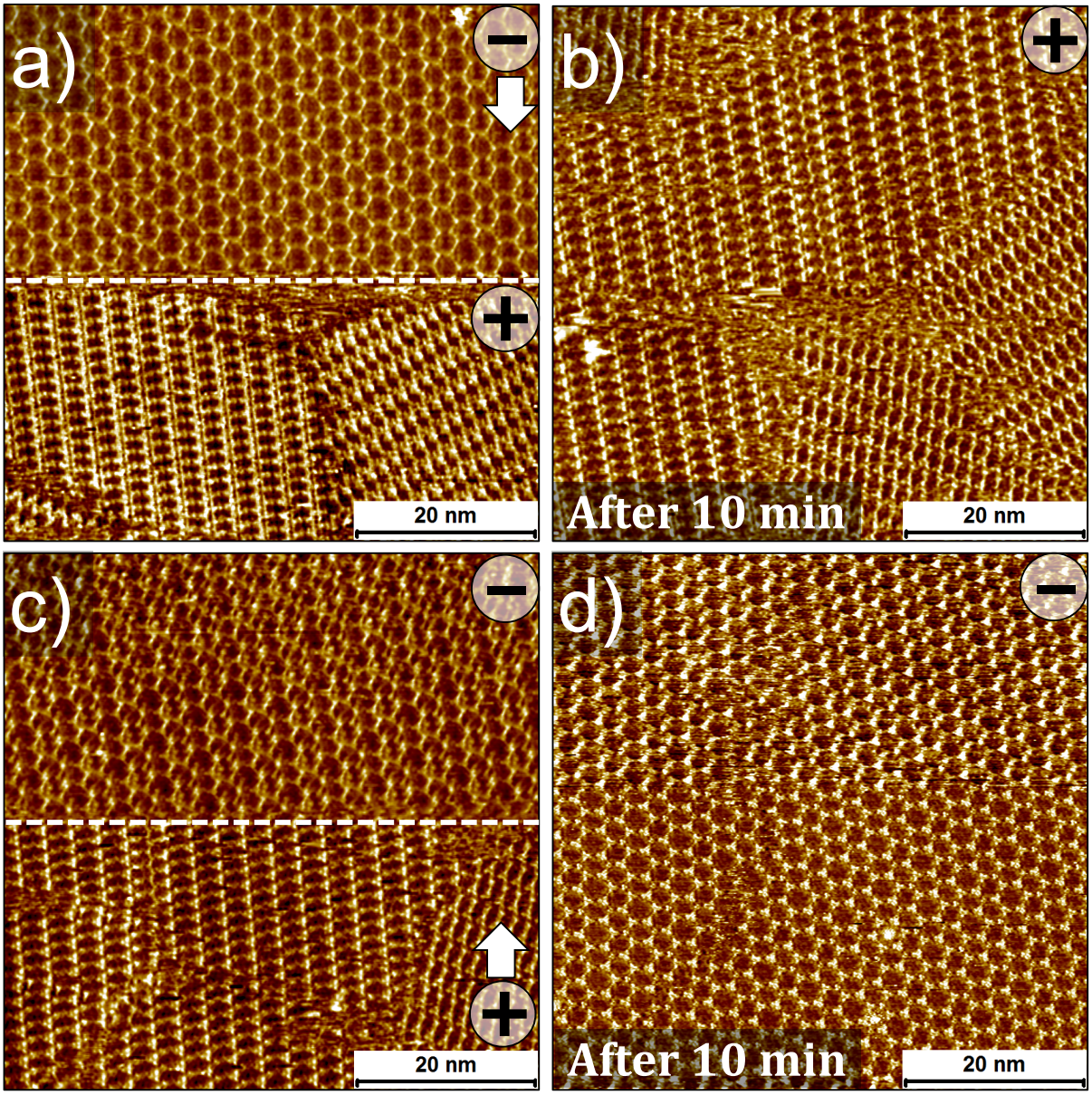

Figure S5. Influence of the reversal of substrate polarity on the mixing behavior studied immediately after and upon 10 minutes of continuous scanning the same area. (a) STM image showing the changes in the structure of 2D co-crystal (C) upon reversing the polarity of the substrate bias from negative to positive, halfway (white dashed line) through the scan while keeping the magnitude of the bias as well as the tunneling current constant. The white arrow in the top-right corner depicts the scan direction. The part of the image scanned at positive substrate bias clearly shows preferential adsorption of **BTB** in the monolayer. (b). STM image showing (approximately) the same area as in (a) scanned further continuously at positive substrate bias. Well-ordered domains of **BTB** are obtained. (c) STM image showing the reverse transition where domains of 2D co-crystal (C) are readily formed upon reversing the polarity. (d) The same area as in (c) scanned further at negative substrate bias. Imaging parameters: I_{set} = 90 pA, V_{bias} = –/+800 mV.

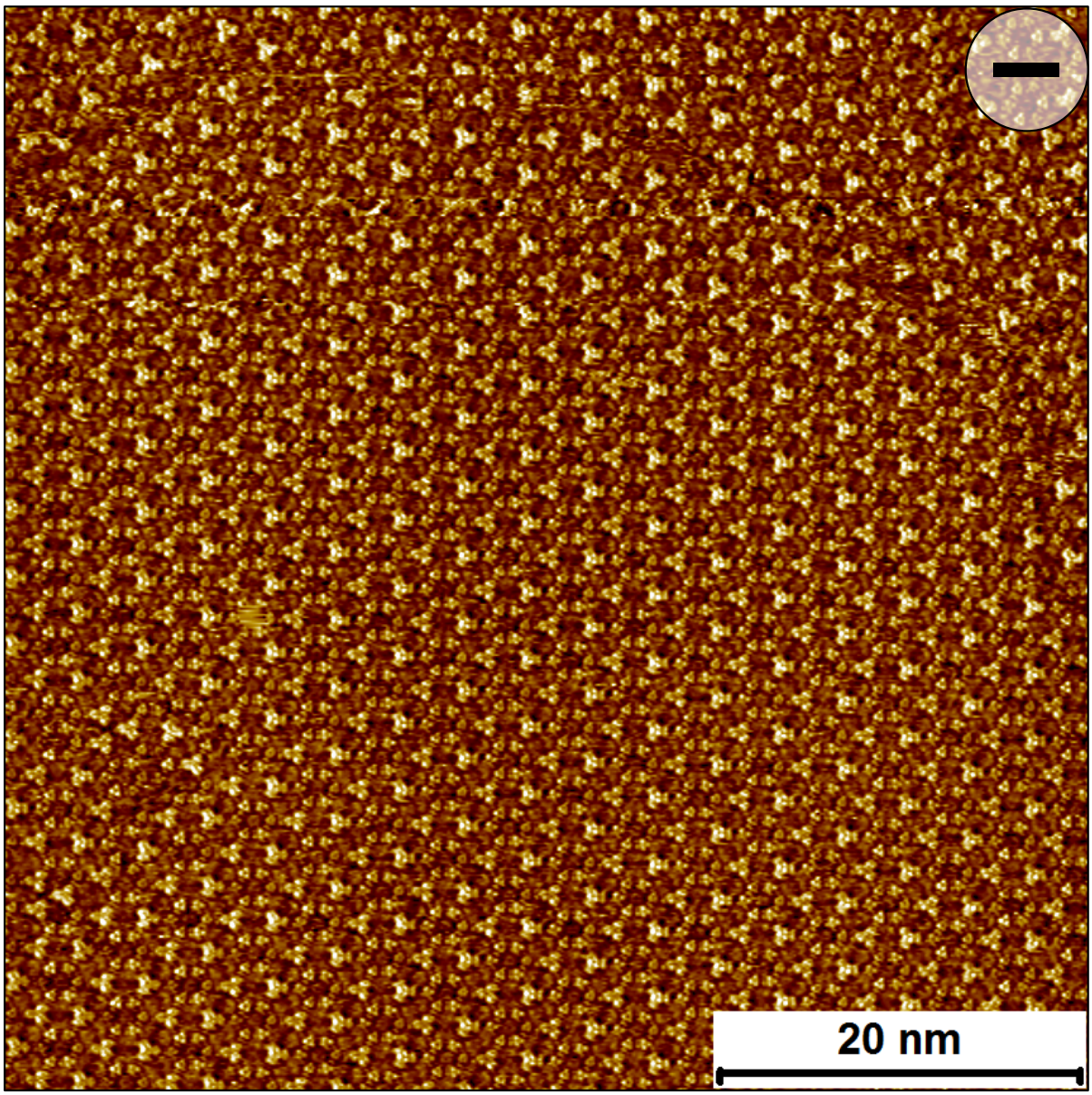

Figure S6. Large-scale STM image of 2D co-crystal (D) formed at negative values of substrate bias. (C_{BTB} = 2.5 X 10^{-4} M and C_{TMA} = 1.7 X 10^{-3} M) Imaging parameters: I_{set} = 90 pA, V_{bias} = –800 mV**.**

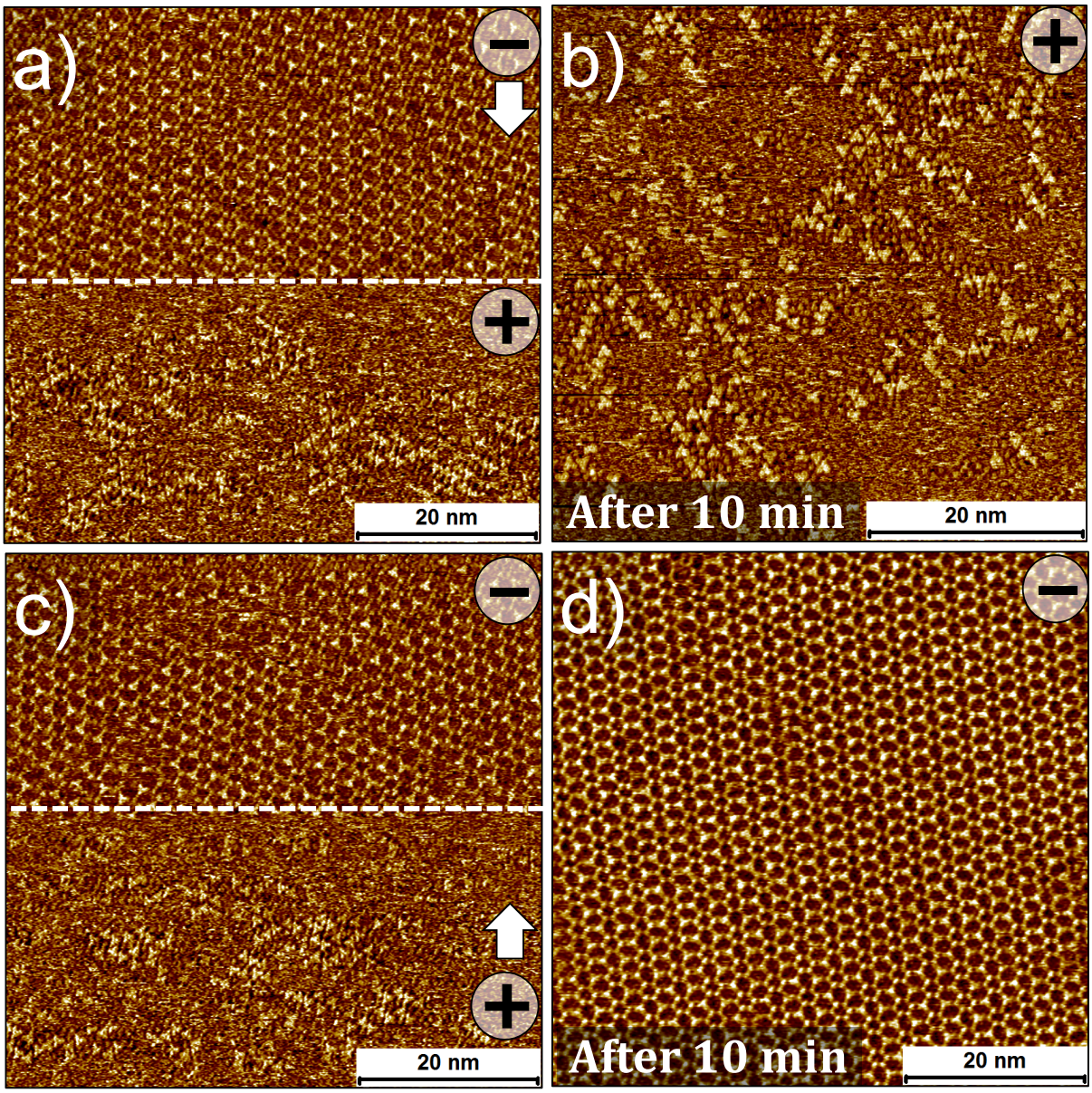

Figure S7. Influence of the reversal of the substrate polarity on the mixing behavior studied immediately after and upon 10 minutes of continuous scanning the same area. (a) STM image showing the changes in the structure of 2D co-crystal (D) upon reversing the polarity of the substrate bias from negative to positive, halfway (white dashed line) through the scan while keeping the magnitude of the bias as well as the tunneling current constant. The white arrow in the top-right corner depicts the scan direction. The part of the image scanned at positive substrate bias shows disordered amorphous network containing both **BTB** as well as **TMA**. (b). STM image showing (approximately) the same area as in (a) scanned further continuously at positive substrate bias. The amorphous network does not show any evolution towards order. (c) STM image showing the reverse transition where domains of 2D co-crystal (D are readily formed upon reversing the polarity. (d) The same area as in (c) scanned further at negative substrate bias. Imaging parameters: I_{set} = 90 pA, V_{bias} = –/+800 mV.

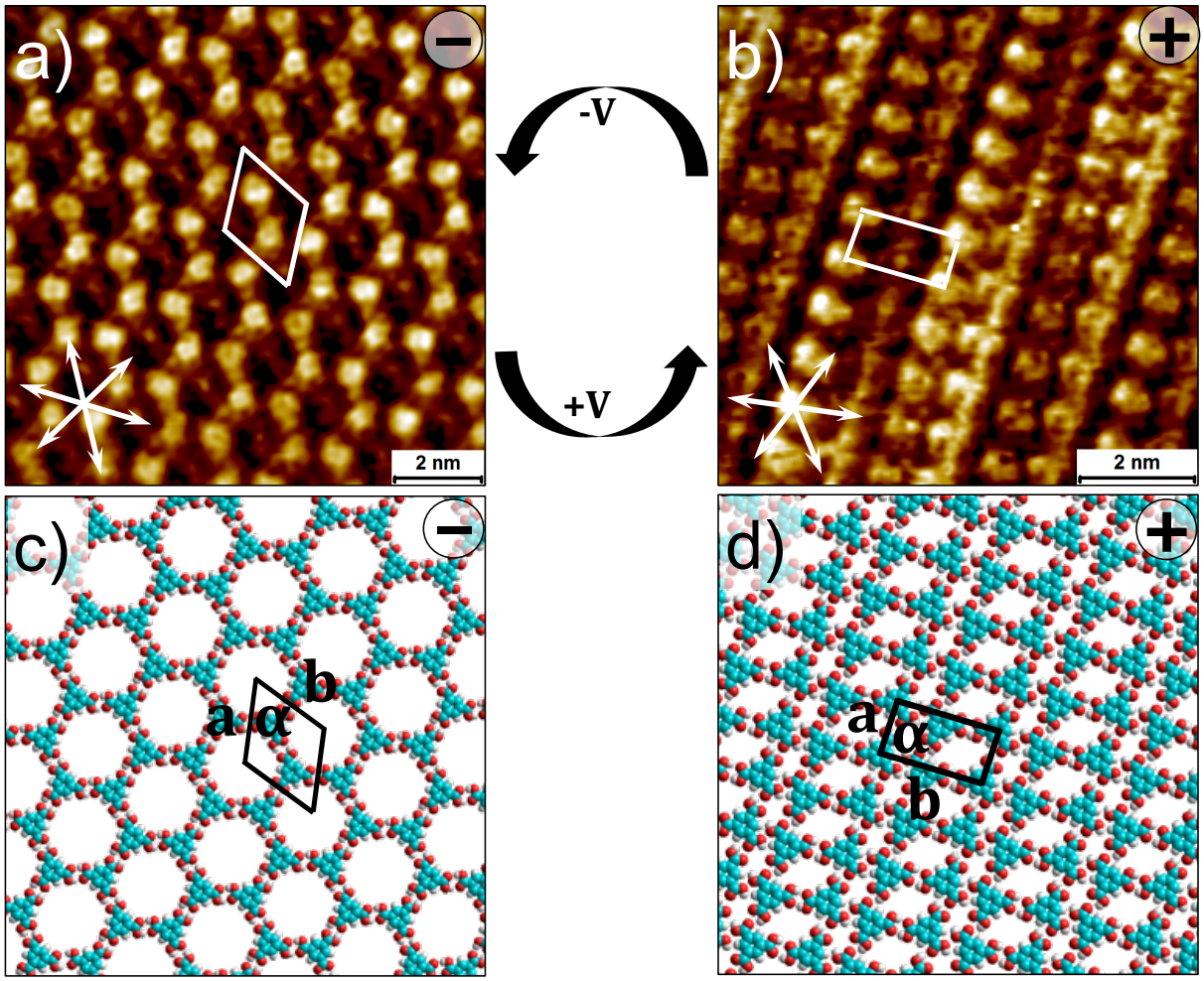

Figure S8. Response of the TMA network to the reversal in the orientation of the EEF. (a) Regular honeycomb network of TMA obtained at negative substrate bias. (b) Compact TMA network obtained at positive substrate bias. Panels (c) and (d) show molecular models corresponding to the STM images provided in (a) and (b), respectively. Imaging parameters: (a) I_{set} = 80 pA, V_{bias} = −1.0 V, (b) I_{set} = 80 pA, V_{bias} = 1.0 V. Unit cell parameters: (a) a = b = 1.7 ± 0.1 nm and α = 60±1.0°. (b) a = 0.9 ± 0.1 nm, b = 1.8 ± 0.1 and α = 86±1.0°

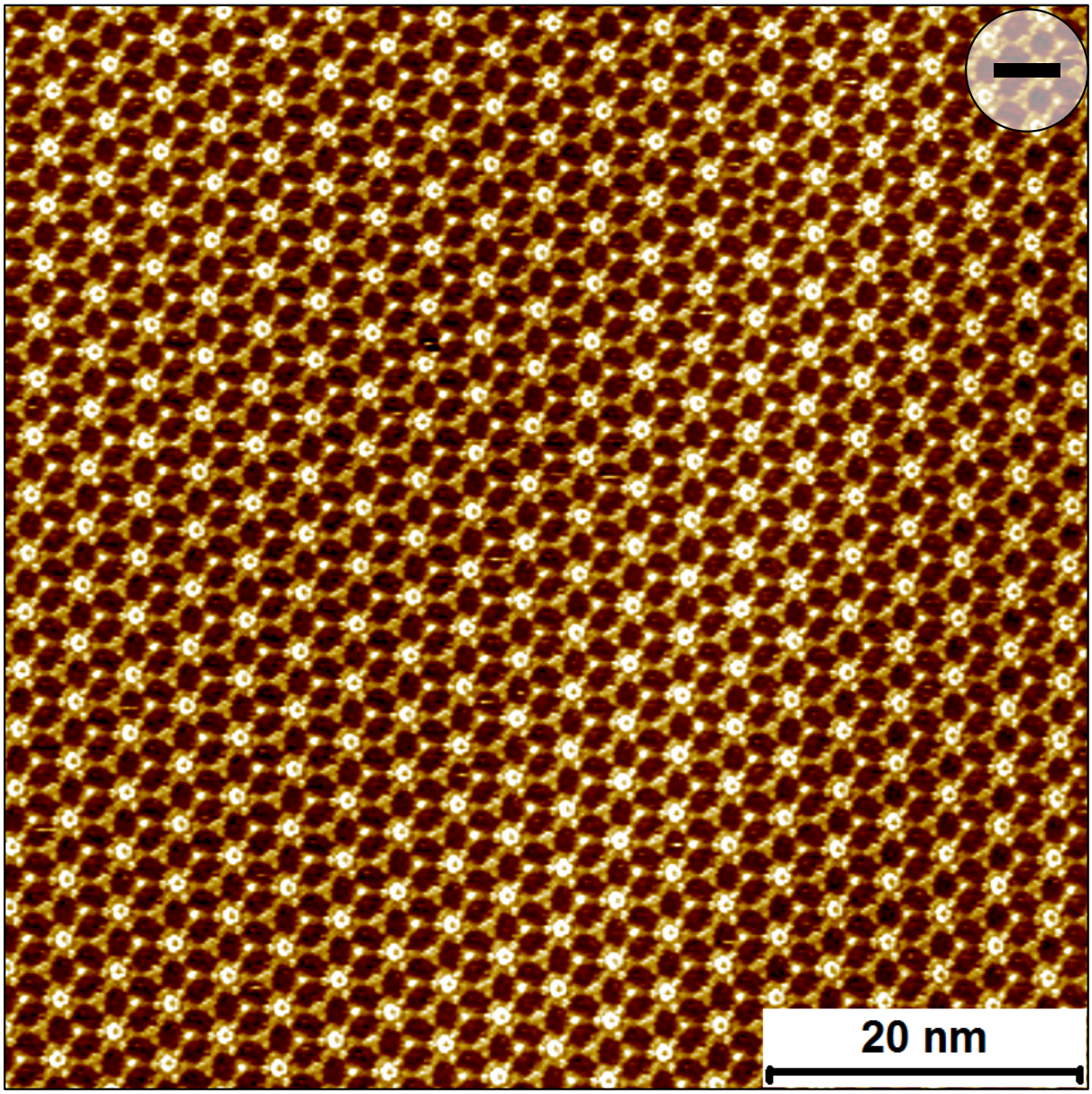

Figure S9. Large-scale STM image of three component system based on host-guest interaction between the 2D co-crystal (D) and **COR** obtained at negative values of substrate bias. To the preformed co-crystal (D) (C_{BTB} = 3.3 x 10^{-4} M, C_{TMA} = 2.3 x 10^{-3} M and C_{COR} = 5.9 x 10^{-4} M) a dilute solution of COR was added.

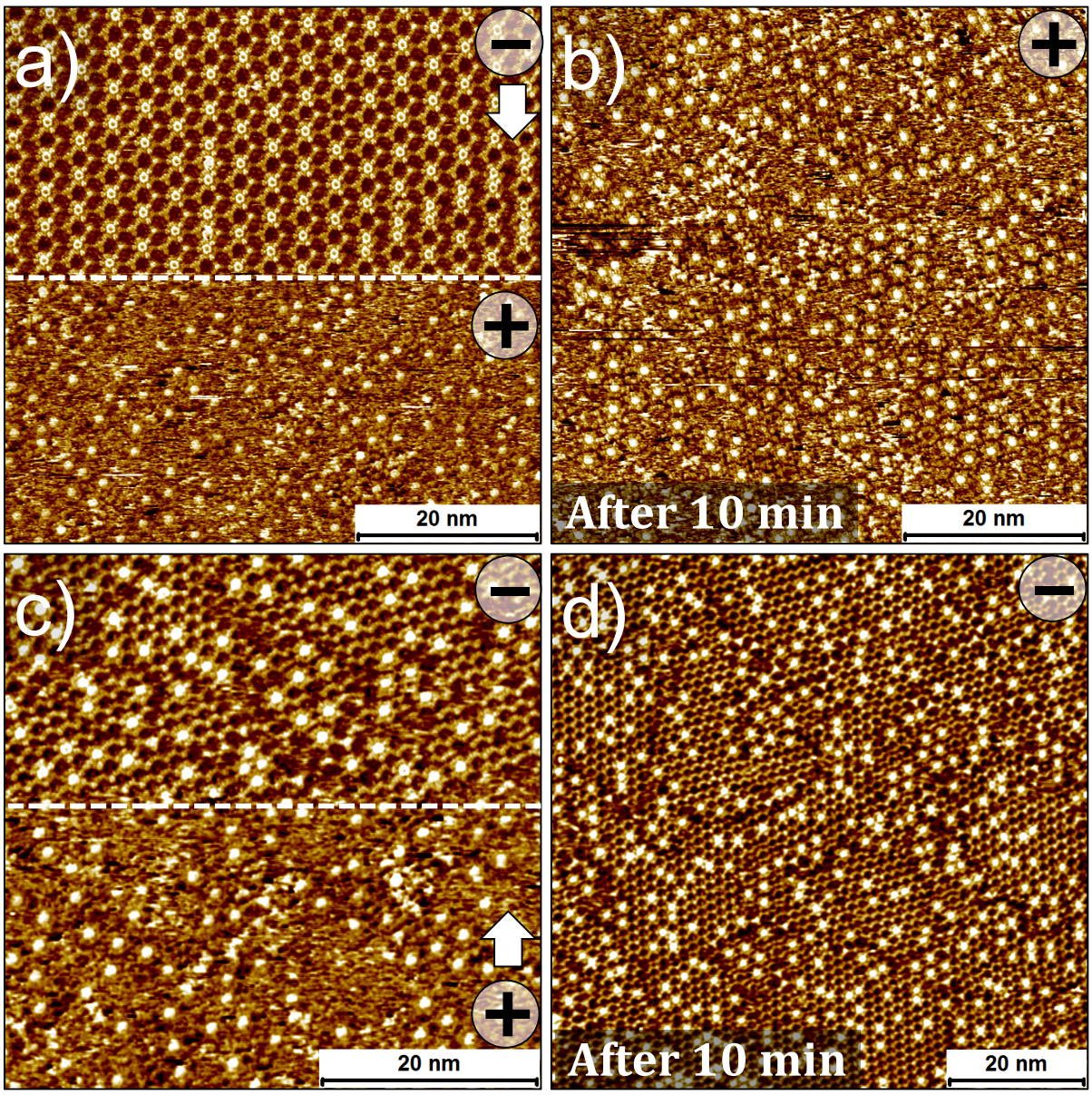

Figure S10. Influence of the reversal of the substrate polarity on the mixing behavior studied immediately after and upon 10 minutes of continuous scanning the same area. (a) STM image showing the changes in the structure of the three-component 2D co-crystal made up of **BTB-TMA-COR** upon reversing the polarity of the substrate bias from negative to positive, halfway (white dashed line) through the scan while keeping the magnitude of the bias as well as the tunneling current constant. The white arrow in the top-right corner depicts the scan direction. The part of the image scanned at positive substrate bias shows disordered network containing **BTB** as well as host guest clusters of **TMA-COR**. (b). STM image showing (approximately) the same area as in (a) scanned further continuously at positive substrate bias. The surface coverage of the **TMA-COR** host-guest system increases. (c) STM image showing the reverse transition where regular honeycomb **TMA-COR** network is formed. (d) The same area as in (c) scanned further at negative substrate bias. Imaging parameters: I_{set} = 100 pA, V_{bias} = –/+900 mV.

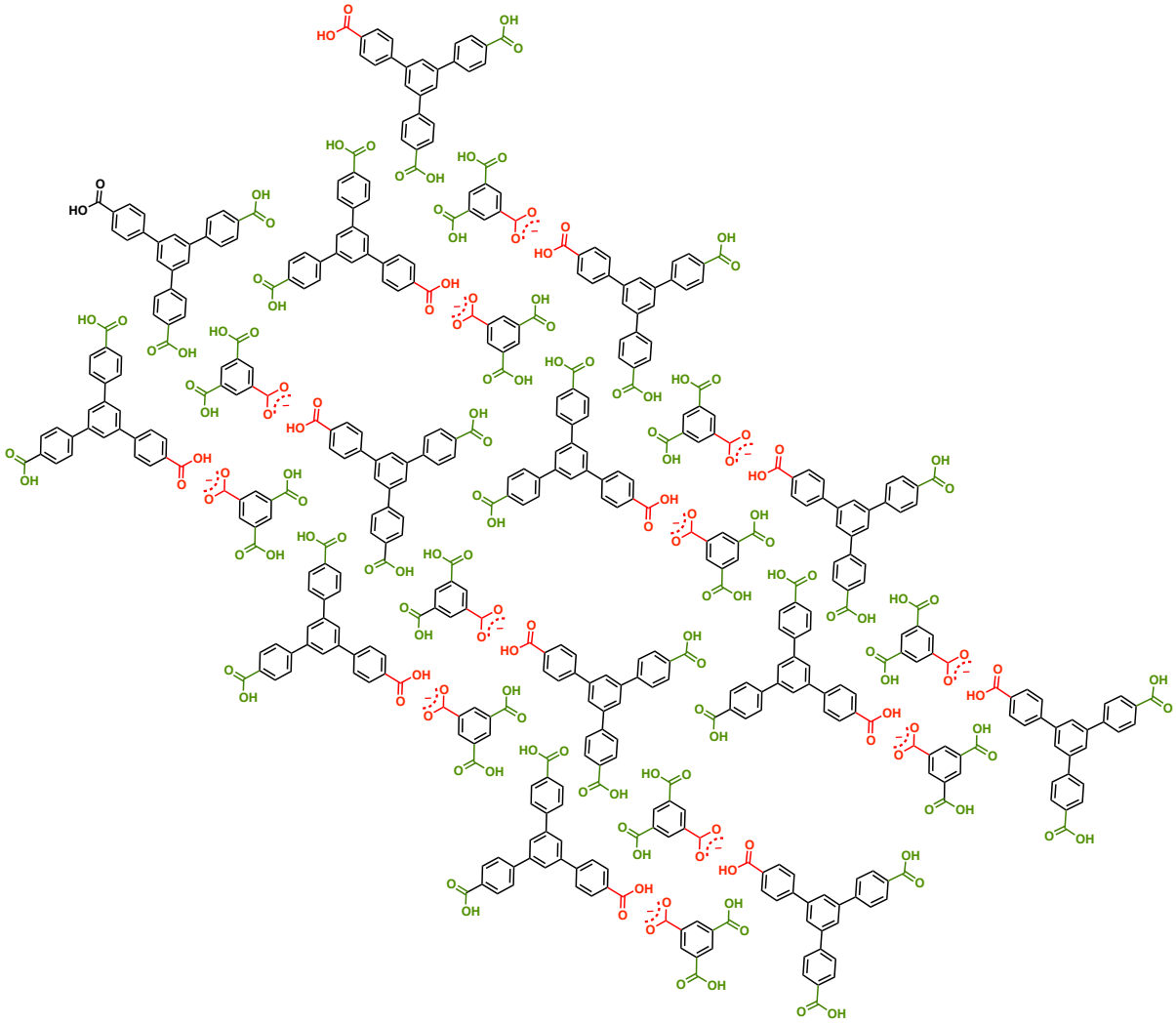

Figure S11. Hypothetical model for 2D co-crystal (B) at positive substrate bias. Note that this network is plausibly sustained by a combination of carboxyl-carboxylate (red) hydrogen bonding together with weak hydrogen bonding between carboxyl-carboxyl and carboxyl aromatic C-H. While this model assumes deprotonation of TMA, it is plausible that both BTB as well as TMA molecules undergo deprotonation.

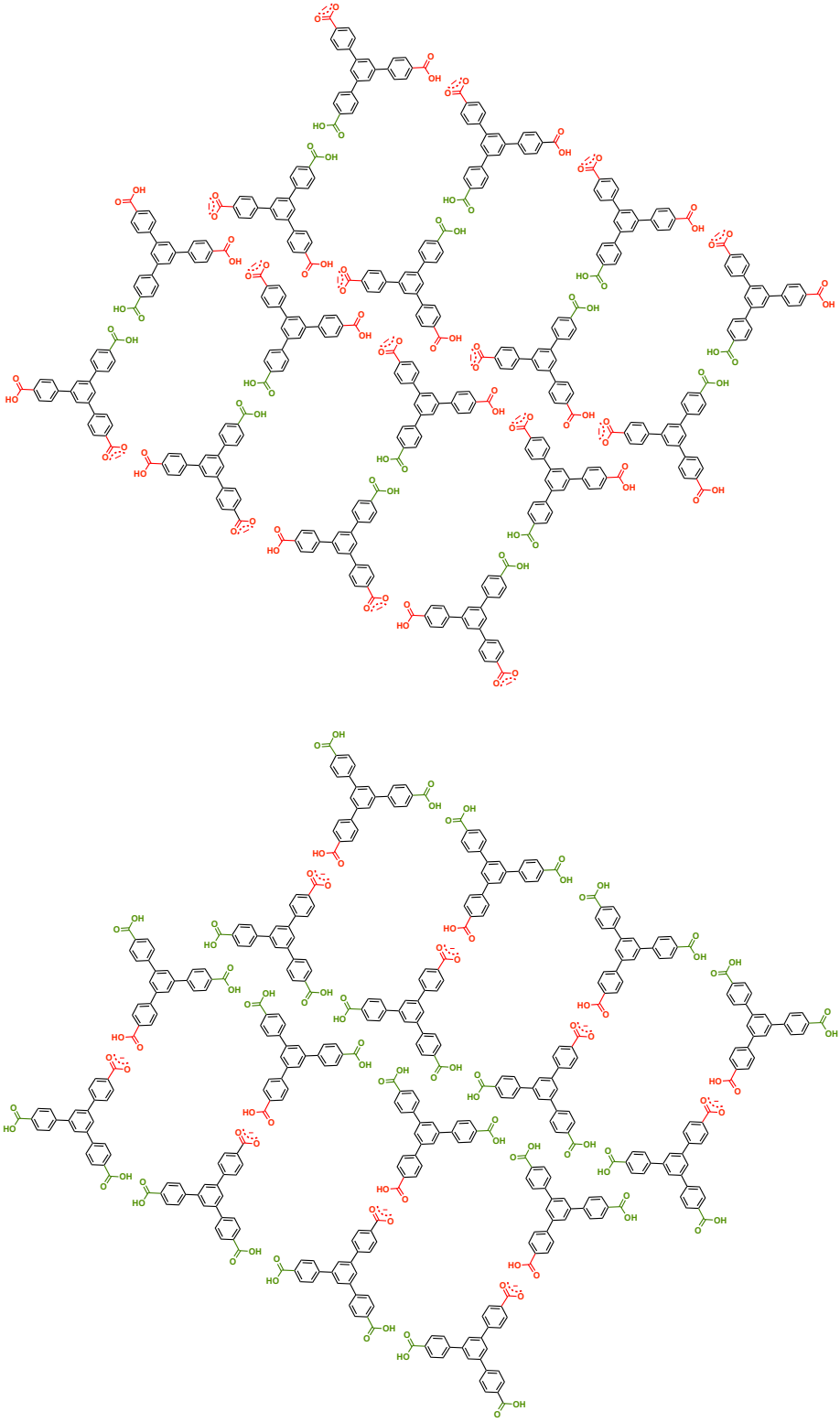

Figure S12. Hypothetical models for the preferentially adsorbed BTB network formed at positive substrate bias. Note that this network is plausibly sustained by a combination of carboxyl-carboxyl (green) and carboxyl-carboxylate (red) hydrogen bonding. Both the models assume a single deprotonation event per BTB molecule.

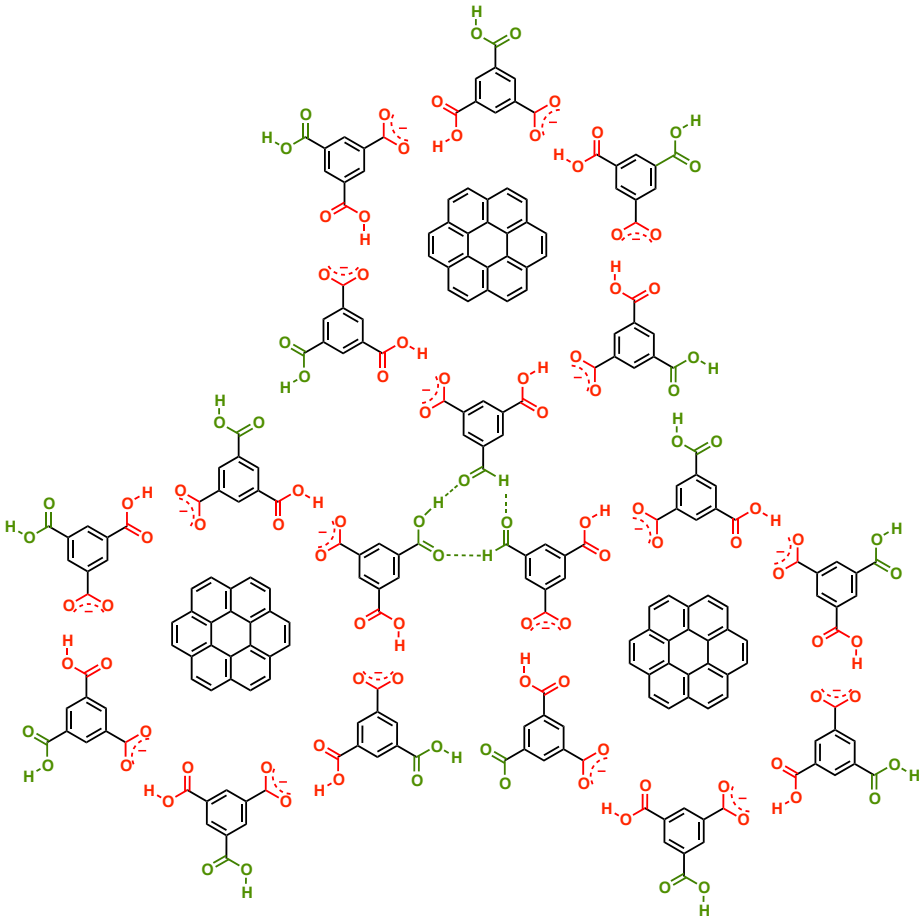

Figure S13. Hypothetical model for the TMA-COR host-guest system formed at positive substrate bias. Note that this network is plausibly sustained by a combination of carboxyl-carboxyl (green) and carboxyl-carboxylate (red) hydrogen bonding. The details of carboxyl-carboxylate hydrogen bonding, the so called low-barrier hydrogen bonding are provided in the main text. The three-fold hydrogen bonding (green) that holds the individual hexagons together has been reported earlier for the TMA network.